

Travelling front solutions in a spatially heterogeneous reaction-diffusion system

M. Chirilus-Bruckner*, L. van Vianen*, F. Veerman*

Abstract

We investigate a two-component reaction-diffusion system with a slow-fast structure and spatially varying coefficients f_1 and f_2 appearing in the slow equation. Under mild boundedness and regularity conditions on f_1 and f_2 the system is shown to exhibit bi-stability in the form of two stable stationary heterogeneous background states. These background states can be connected by stationary and travelling front solutions. Travelling fronts feature an interface that moves with a non-uniform speed through the motionless spatially varying background states it connects. We construct both the background states and stationary fronts using an extension of Fenichel theory to the non-compact case. Additionally, we establish the existence of travelling front solutions and derive a leading-order expression for the dynamic position of the moving interface through a time-dependent spatial dynamics approach. This expression takes the form of a delay-differential equation, and its accuracy is validated through numerical simulations. A key contribution of our work lies in the general treatment of f_1 and f_2 , which are neither (necessarily) asymptotically small nor restricted to specific forms such as periodic or localized structures. Furthermore, our derivation of the front position formula circumvents the traditional reliance on spectral analysis, enabling us to describe front dynamics beyond bifurcations from stationary fronts. This approach has the potential to be extended to other settings in which spectral properties at onset preclude conventional reduction techniques.

Contents

1	Introduction	2
1.1	Main results and Plan of the paper	3
1.2	Numerical illustration of travelling front solutions	3
1.3	Related work and novelty of the present work	5
2	Stationary background states	6
3	Front solutions	10
3.1	Stationary front solutions	10
3.2	Travelling fronts with non-zero speed	12
3.2.1	Initialised travelling fronts	12
3.2.2	Entire travelling front solutions	15
4	Delay-differential equation for front position dynamics	18
4.1	Formal derivation	18
4.2	Numerical algorithm for the delay-differential equation	23
4.2.1	Algorithm 1	24
4.2.2	Algorithm 2	25
4.2.3	Algorithm 1 vs Algorithm 2	25
4.3	Numerical exploration of front dynamics	25
5	Summary and outlook	39

*Mathematical Institute, Leiden University, Einsteinweg 55, 2333 CC, Leiden, the Netherlands

1 Introduction

We consider travelling front solutions of the reaction-diffusion equation

$$\begin{cases} \partial_t U = \varepsilon^2 \partial_x^2 U + U - U^3 - \varepsilon(\alpha V + \gamma), \\ \tau \partial_t V = \partial_x^2 V - [1 + f_1(x)]V + [1 + f_2(x)]U, \end{cases} \quad (1.1)$$

with parameters $\alpha, \gamma \in \mathbb{R}$, $\tau > 0$, perturbation parameter $0 < \varepsilon \ll 1$ and spatially varying coefficients f_1 are f_2 that are not necessarily assumed to be small or with a specific structure (e.g. periodic or localized).

Assumptions 1.1. *Let the coefficients $f_k, k = 1, 2$ in (1.1) fulfil the following:*

- $f_k \in C_b^3(\mathbb{R})$, i.e. f_k is bounded and sufficiently smooth, and
- $\inf_{x \in \mathbb{R}} [f_k(x) + 1] > 0$.

The present work establishes that (1.1) exhibits bi-stability, characterized by two stable stationary background states that vary in space due to the presence of f_1, f_2 and further give rise to stationary and travelling front solutions that connect them (see Figure 1).

Background: Nagumo/Allen-Cahn setting. Consider the Nagumo equation

$$\partial_t U = \varepsilon^2 \partial_x^2 U + U - U^3 - \varepsilon \gamma.$$

Provided that ε and γ are such that $u - u^3 + \varepsilon \gamma = 0$ has three distinct real roots, it has three constant background states $u^-(\varepsilon) < u^0(\varepsilon) < u^+(\varepsilon)$ with $u^\pm(\varepsilon) = \pm 1 - \frac{\gamma}{2}\varepsilon + \mathcal{O}(\varepsilon^2)$, $u^0(\varepsilon) = \gamma\varepsilon + \mathcal{O}(\varepsilon^2)$. Furthermore, it features uniformly moving front solutions

$$U_{TF}(x, t) = u_{*,+}(\varepsilon) + u_{*,-}(\varepsilon) \tanh \left[\sqrt{2} u_{*,-}(\varepsilon) \left(\frac{x - \varepsilon^2 c(\varepsilon) t}{2\varepsilon} \right) \right],$$

with $u_{*,\pm}(\varepsilon) = (u^\pm(\varepsilon) \pm u^0(\varepsilon))/2$ whose speed is given by $c(\varepsilon) = -(u^+(\varepsilon) - 2u^0(\varepsilon) + u^-(\varepsilon))/(\sqrt{2}\varepsilon) = \frac{3}{\sqrt{2}}\gamma + \mathcal{O}(\varepsilon)$. In particular, if $\gamma = 0$ there are only stationary front solutions and the forcing $\varepsilon\gamma$ induces the movement.

Background: Constant-coefficient reaction-diffusion model. A similar structure is inherited by the constant-coefficient version of (1.1)

$$\begin{cases} \partial_t U = \varepsilon^2 \partial_x^2 U + U - U^3 - \varepsilon(\alpha V + \gamma), \\ \tau \partial_t V = \partial_x^2 V - V + U. \end{cases} \quad (1.2)$$

It has stable background states $(u, v)^\pm(\varepsilon) = \pm(1, 1) + \mathcal{O}(\varepsilon)$ that can be connected by stable stationary, uniformly travelling and dynamically travelling front solutions (cf. [7, 8, 9]). More specifically, travelling front solutions $(U, V)(x, t) = (u_{\text{tf}}, v_{\text{tf}})(x - \varepsilon^2 ct)$ exist if the leading order existence condition

$$\alpha v_* + \gamma = \frac{\sqrt{2}}{3} c, \quad v_* := \frac{c \hat{\tau}}{\sqrt{c^2 \hat{\tau}^2 + 4}}, \quad (1.3)$$

relating the speed $c \in \mathbb{R}$ and the system parameters is fulfilled. Notably, we assumed a "large" relaxation parameter $\tau =: \frac{\hat{\tau}}{\varepsilon^2} > 0$. This shows, in particular, that if τ is not large enough, so $\hat{\tau} = 0$, then the second component does not impact the front motion. Moreover, from [11, 17, 19] multi-front and pulse solutions of (1.2) are known to have particularly rich dynamics in this regime.

Fast-reaction scaling. Given the role of $\tau = \frac{t}{\varepsilon^2} > 0$ for the constant-coefficient setting we choose to stick to this parameter choice throughout this article which, in fact, can be related via $s = \varepsilon^2 t$ to the fast-reaction limit ([29, 36, 37])

$$\begin{cases} \varepsilon^2 \partial_s U = \varepsilon^2 \partial_x^2 U + U - U^3 - \varepsilon(\alpha V + \gamma), \\ \hat{\tau} \partial_s V = \partial_x^2 V - [1 + f_1(x)]V + [1 + f_2(x)]U. \end{cases} \quad (1.4)$$

1.1 Main results and Plan of the paper

The first main contribution is to prove that, under the mild Assumptions 1.1, the PDE admits two stable stationary heterogeneous background states $(u_b^\pm(x; \varepsilon), v_b^\pm(x; \varepsilon))$. Their rigorous construction is sketched in Section 2. Adopting a spatial-dynamics viewpoint, we analyse the steady-state ODE, augmented by the additional variable $\chi_x = 1$, which features critical and slow manifolds that are non-compact. We sketch an extension of classical Fenichel theory to the non-compact setting and prove the existence of two bounded solutions that correspond to the two heterogeneous background states in the PDE, which are shown in [39] to be stable.

The second main contribution, given in Section 3, is existence theory for front solutions connecting these motionless backgrounds. Stationary fronts are obtained in Section 3.1 as heteroclinic connections between the two bounded solutions of the steady-state ODE from Section 2, using a Melnikov-type computation that yields a leading-order existence and selection condition fixing admissible front locations, reflecting the loss of translation invariance caused by heterogeneity. Building on this, we further establish in Section 3.2 the existence of genuinely travelling fronts whose interface moves with non-uniform speed through stationary heterogeneous tails given by the heterogeneous background states from Section 2. We sketch the rather lengthy rigorous construction from [39], in which one first controls the initial-value problem with carefully defined “initialised fronts” and then tracks the evolution of the time derivatives $(\partial_s U, \partial_s V)$, which decay to zero in the far field since the backgrounds do not move. We round off our exposition with Section 4, where we derive a reduced law for the motion of the interface of travelling front solutions. In the singular limit $\varepsilon \rightarrow 0$, the front position $z(s)$ satisfies a delay-differential equation in which the instantaneous drift $z'(s)$ depends on a history-dependent functional $W[z]$ arising from solving an auxiliary linear parabolic problem for the slow field. Crucially, this reduction is obtained without spectral analysis, allowing front-dynamics descriptions beyond bifurcations from stationary fronts. Numerical simulations validate the leading-order delay law and illustrate regimes including heterogeneous speed modulation, attraction and repulsion by stationary fronts for $\alpha < 0$, and exploratory dynamics outside the strict assumptions.

Throughout this paper, we present the main results from [39] as ‘Results’ rather than ‘Theorems’, as this paper does not contain the proof of those results. All Results presented here correspond to Theorems in [39], whose proof can be found therein.

1.2 Numerical illustration of travelling front solutions

Before embarking on a journey to study (1.1) analytically, we briefly show the U - and V -profiles of travelling front solutions along with a density plot showing the corresponding position $z = z(t)$, which is defined as the unique zero of the U -component (see Definition 3.8). Much of the analytical set-up is, in fact, inspired by careful observations of numerical simulations. In particular, the motionless background states of travelling

fronts has been first discovered numerically. In Figure 1 we show a traveling front for

$$\begin{aligned}
 f_1(x) &= 4 + e^{-(x-150)^2}, & f_2(x) &= 3 + 0.8g(x), \\
 g(x) &= e^{-(x-50)^2} - e^{-(0.1(x-80))^2} + e^{-(0.05(x-120))^2} - e^{-(0.05(x-200))^2} + 2e^{-(0.05(x-240))^2} \cos(1.5x) + 0.5 \cos((0.04x)^2)
 \end{aligned}
 \tag{1.5}$$

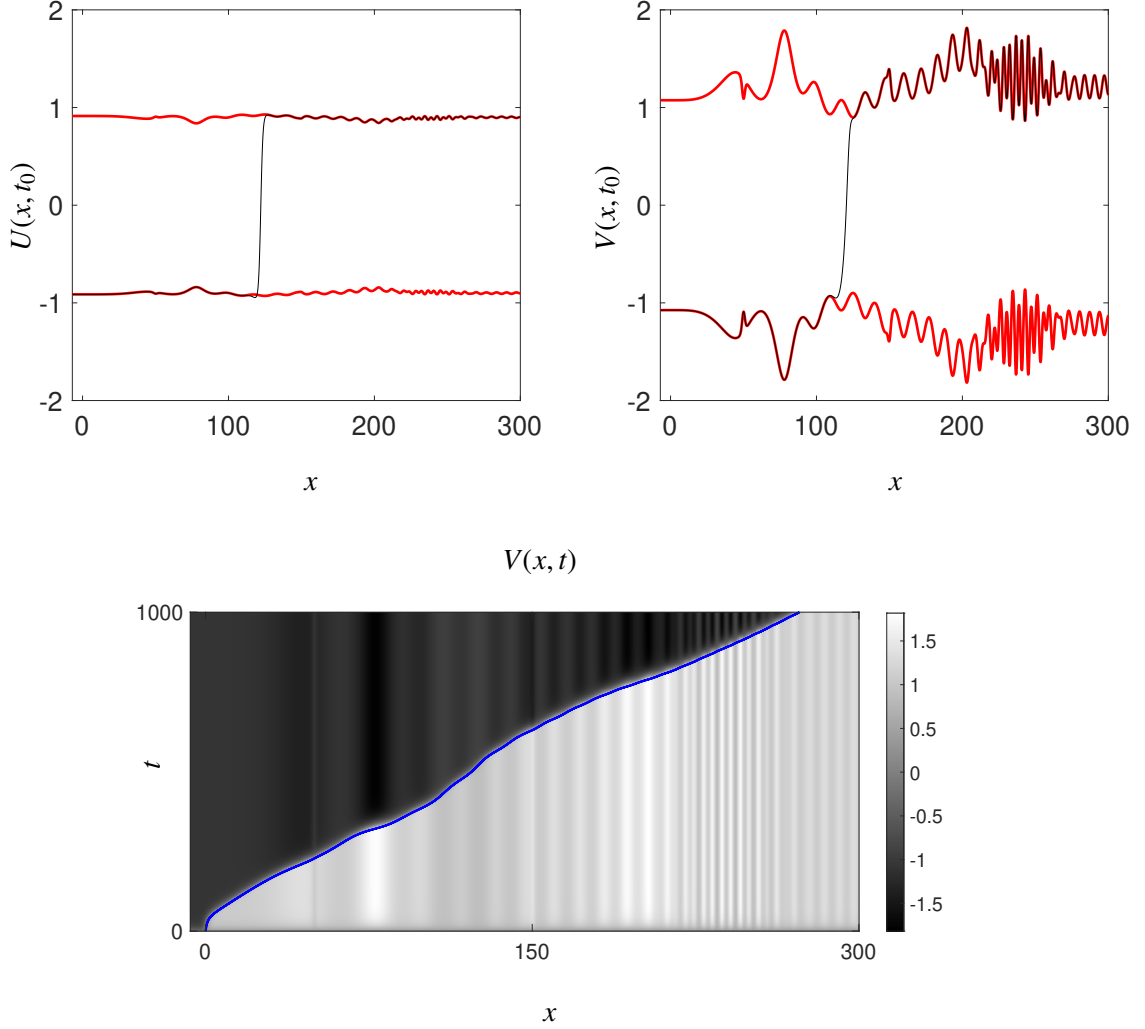


Figure 1: Numerical computation of solutions of (1.1). **Upper panels.** Snapshot in time of the (black) U -profile along with (red) background states (left upper panel) and (black) V -profile along with (red) background states (right upper panel). **Lower panel.** Density plot for the V -profile along with (black) position $z(t)$, defined by the unique zero of the U -component, see Definition 3.8. **Details of numerical computation.** Coefficients f_1, f_2 from (1.5); Initial Conditions: $u(x, 0) = \tanh(x/\varepsilon), v(x, 0) = 0.1$; Boundary conditions: homogeneous Neumann; Parameter settings: $\varepsilon = 0.15, \alpha = 0.94, \gamma = 0, \hat{\tau} = 1$. Numerical solver: MATLAB (2020): "pdepe". Code is available at [6]

1.3 Related work and novelty of the present work

The transition from (1.2) to (1.1) is motivated by prior work on a related reaction-diffusion equation, namely, the extended Klausmeier model with spatially varying coefficients, which is used to model the dynamics of vegetation patterns in semi-arid regions where the spatially varying coefficients account for the change in topography (cf. [3]). This further generalised previous studies which assumed the terrain to be either flat or with a constant slope ([35]). The novelty in [3] consisted in using a blend of Geometric Singular Perturbation Theory (GSPT) and the theory of exponential dichotomies to construct spatially varying background states and stationary pulse solutions that are bi-asymptotic to those for $x \rightarrow \pm\infty$. These new types of pulse solutions with heterogeneous tails model vegetation patches on varying topography. Going beyond the stationary case, a reduced description of the position of travelling vegetation patterns was given consisting of a coupled ODE-algebraic system that described the drift instability of stationary pulses. While similar in methodology to [3], the study of front solutions of (1.1) in the present work poses several new challenges whose resolution will allow to generalize the approach to a larger class of equations. We will comment on those throughout the text.

Going beyond the dynamics of single vegetation patches, the influence of heterogeneity on N -pulse (also sometimes called N -spike) solutions has been studied by a reduction procedure to a finite-dimensional systems of ODEs, e.g. in [4] and [26]. Furthermore, the limit of small-amplitude vegetation patterns on spatially periodic terrains has been studied in paradigm models such as the Swift-Hohenberg equation [30, 24] by deriving a Ginzburg-Landau equation for the pattern amplitude. In [31] even the idea of reversing desertification via resonance with a spatially periodic forcing coefficient was presented.

For scalar Nagumo/Allen-Cahn-type settings, in [32] and [5] the influence of heterogeneity on front and multi-front solutions has been studied. Related results can be also found in [34] for the Allen-Cahn with forcing and discrete versions thereof. Going back to reaction-diffusion systems, in [18] a three-component model of the form (1.2) was studied with $\gamma = \gamma(x)$ a step function. All of these settings can be viewed as complementary results to the present work, since they explain how heterogeneity influences primarily the fast variable U .

The influence of heterogeneity on pattern formation in 2-D is a very active research field with many applications including to universal phenomena like the formation of Turing patterns or spiral waves. We refrain from giving an extensive list, but rather point to two bodies of work that contain a wealth of analytical results and techniques: [25], [22], [20], [23], [21] and also [38],[28], [27]. All these settings have many similarities with (1.1) and will serve as an inspiration for future work.

2 Stationary background states

To study the existence of front solutions in (1.1), we first have to determine the existence of stationary background states that can be connected with via a front – in other words, to which the front is bi-asymptotic as $x \rightarrow \pm\infty$.

Result 2.1. *Let f_1 and f_2 satisfy Assumptions 1.1. Then there exists $\varepsilon_0 > 0$ such that for all $0 \leq \varepsilon \leq \varepsilon_0$ system (1.1) has a pair of bounded stationary solutions $(u_b^\pm(x; \varepsilon), v_b^\pm(x; \varepsilon))$ that satisfy*

$$\inf_{\varepsilon \in [0, \varepsilon_0]} \inf_{x \in \mathbb{R}} u_b^+(x; \varepsilon) > 0 \text{ and } \sup_{\varepsilon \in [0, \varepsilon_0]} \sup_{x \in \mathbb{R}} u_b^-(x; \varepsilon) < 0,$$

$$\inf_{\varepsilon \in [0, \varepsilon_0]} \inf_{x \in \mathbb{R}} v_b^+(x; \varepsilon) > 0 \text{ and } \sup_{\varepsilon \in [0, \varepsilon_0]} \sup_{x \in \mathbb{R}} v_b^-(x; \varepsilon) < 0.$$

Furthermore, $u_b^\pm(\cdot; \varepsilon) \in C_b^7(\mathbb{R})$, $v_b^\pm(\cdot; \varepsilon) \in C_b^5(\mathbb{R})$, $u_b^\pm(x; 0) = \pm 1$. Suppose $f_1 = 0$. Using the solution operator

$$G(\phi)(x) := e^{-x} \int_{-\infty}^x \frac{1}{2} e^\xi \phi(\xi) d\xi + e^x \int_x^\infty \frac{1}{2} e^{-\xi} \phi(\xi) d\xi, \quad (2.1)$$

we have that

$$v_b^\pm(x; 0) = \pm G(1 + f_2)(x) = \pm e^{-x} \int_{-\infty}^x \frac{1}{2} e^\xi (1 + f_2(\xi)) d\xi \pm e^x \int_x^\infty \frac{1}{2} e^{-\xi} (1 + f_2(\xi)) d\xi. \quad (2.2)$$

Remark 2.2. For a general version of (2.2) for nonzero f_1 , see [39, Chapter 3]

Remark 2.3. We observe that if $f_2 = 0$ then $v_b^\pm = \pm 1$. Furthermore, the result holds equally for non-zero f_1 with the small change that (2.2) will feature a fundamental system of $v'' - (1 + f_1(x))v = 0$ instead of exponentials. Notice also that, to leading order, the effect of f_k is only visible in the v -component.

Result 2.1 is stated as a Theorem in [39, Chapter 3], where its full proof can be found. We omit the details of this proof here, and provide an outline of the proof structure. The proof of Result 2.1 is based on the study of the ODE system

$$\begin{aligned} \varepsilon u_x &= p, \\ \varepsilon p_x &= -u + u^3 + \varepsilon(\alpha v + \gamma), \\ v_x &= q, \\ q_x &= (1 + f_1(\chi))v - (1 + f_2(\chi))u, \\ \chi_x &= 1. \end{aligned}$$

We are interested in finding background orbits $\text{BO}_\varepsilon^\pm$ of (2.3) for $0 \leq \varepsilon \ll 1$ (the singular limit $\varepsilon = 0$ included where (2.3) becomes a DAE, i.e. a differential algebraic equation), which are characterized by imposing that the (u, p, v, q) components are bounded, and that the (u, p) components are $\mathcal{O}(\varepsilon)$ close to $(\pm 1, 0)$. The usual path for analysis in case $f_k = 0$ would be to exploit the slow-fast structure that gives rise to a critical manifold of which only a compact subset is considered. A similar approach for non-zero f_k leading to the system (2.3) already poses the first difficulty, since one now cannot restrict to compact subsets of the critical manifold, so standard Fenichel theory [13, 14, 15] cannot be applied directly. Instead, the proof in [39] combines the approach of

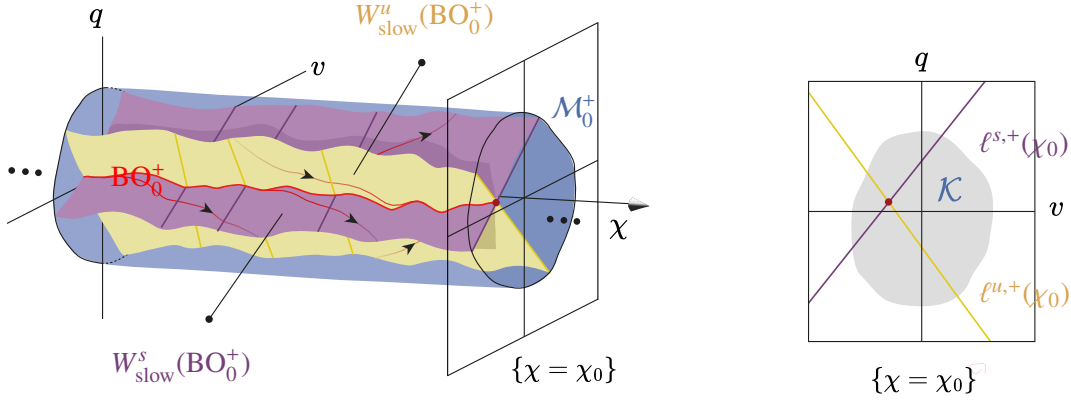


Figure 2: A visualisation of the reduced slow dynamics in a neighbourhood of BO_0^+ in the hyperplane $\{u = +1, p = 0\}$. Left: the manifold \mathcal{M}_0^+ in black, the singular bounded orbit BO_0^+ in red, the slow unstable manifold of BO_0^+ in purple, the slow stable manifold of BO_0^+ in yellow. Right: the intersection with the hyperplane $\{\chi = \chi_0\}$, with the line $\ell^{u,+}(\chi_0)$ in purple and $\ell^{s,+}(\chi_0)$ in yellow; the compact set \mathcal{K} is indicated in gray.

[13, 15] with the results on exponential dichotomies found in [16]. In the singular limit $\varepsilon = 0$, the existence of a pair of (reduced) background orbits $BO_{0,R}^\pm$ in the slow reduced system

$$\begin{aligned} v_x &= q, \\ q_x &= [1 + f_1(\chi)]v \pm [1 + f_2(\chi)], \\ \chi_x &= 1 \end{aligned}$$

for $u = \pm 1$ is shown using the existence of an exponential dichotomy in the homogeneous equation $v_{xx} = [1 + f_1]v$, which is equivalent to the Riccati equation $a^2 + a_x = 1 + f_1(x)$. The background orbit for $\varepsilon = 0$ is given by $BO_0^\pm := \{u = \pm 1, p = 0\} \times BO_{0,R}^\pm$.

Remark 2.4. Note that if the slow variable v were to satisfy a more general linear system one could still use the theory of exponential dichotomies as in [10, 3] with the drawback that one then needs to enforce a (additional) bound on f_1 which the Riccati equation for the special case of $v_{xx} = (1 + f_1)v$ circumvents. The existence of orbits BO_0^\pm to (2.4) then follows, cf. [10, Prop.2, Ch.8].

Note that, for $f_1 \equiv 0$, the v -component of the orbit BO_0^\pm yields the solution $v_b^\pm(x; 0)$ as given in Result 2.1. The persistence of the orbits BO_0^\pm for $0 \leq \varepsilon \ll 1$ in the full system (2.3) is proved using the following steps. First, we define the manifolds

$$\mathcal{M}_0^\pm := \{u = \pm 1, p = 0, (v, q) \in \mathcal{K}, \chi \in \mathbb{R}\}, \quad (2.5)$$

with $\mathcal{K} \subset \mathbb{R}^2$ a compact set in (v, q) -space chosen sufficiently large to (at least) contain the appropriate singular background orbit

$$BO_0^\pm := \{u = \pm 1, p = 0\} \times \bigcup_{\chi \in \mathbb{R}} (v_b^\pm(\chi; 0), q_b^\pm(\chi; 0), \chi), \quad q_b^\pm = \frac{dv_b^\pm}{dx}. \quad (2.6)$$

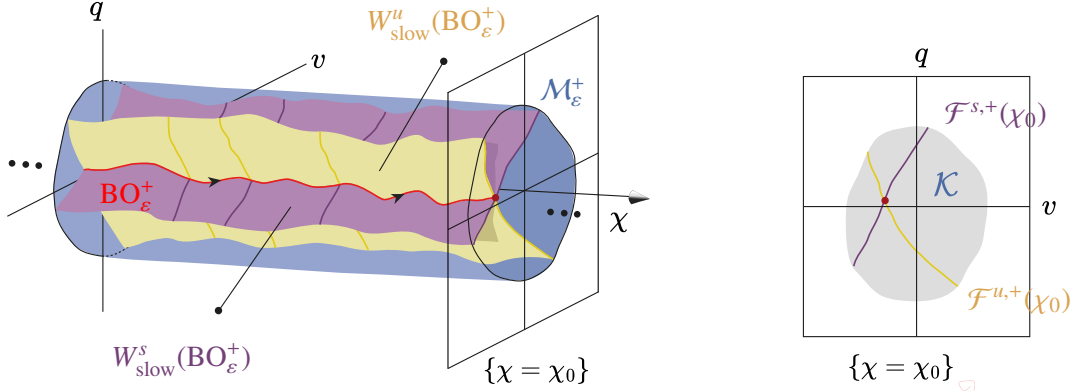


Figure 3: A visualisation of the slow dynamics in a neighbourhood of BO_ε^+ near the hyperplane $\{u = +1, p = 0\}$. Left: the manifold $\mathcal{M}_\varepsilon^+$ in black, the background orbit BO_ε^+ in red, the slow unstable manifold of BO_ε^+ in purple, the slow stable manifold of BO_ε^+ in yellow. Right: the intersection with the hyperplane $\{\chi = \chi_0\}$, with the fibre $\mathcal{F}^{u,+}(\chi_0)$ in purple and $\mathcal{F}^{s,+}(\chi_0)$ in yellow; the compact set \mathcal{K} is indicated in gray.

The slow stable and unstable manifolds of BO_0^\pm (defined as the stable and unstable manifolds of $\text{BO}_{0,R}^\pm \subseteq \mathcal{M}_0^\pm$) (2.4) are foliated by a family of lines $\ell^{u/s,\pm}(\chi)$, see Figure 2, i.e.

$$W_{\text{slow}}^{u/s}(\text{BO}_0^\pm) = \bigcup_{\chi \in \mathbb{R}} \ell^{u/s,\pm}(\chi). \quad (2.7)$$

The manifolds \mathcal{M}_0^\pm are normally hyperbolic, which is immediately apparent from the fast (u, p) -dynamics in (2.3). This allows us to define the (fast) local stable and unstable manifolds of \mathcal{M}_0^\pm ,

$$W^{u/s}(\mathcal{M}_0^\pm) = \left\{ u \in \mathcal{U}^\pm, p = -\frac{1-u^2}{\sqrt{2}} \text{ (stable) or } p = \frac{1-u^2}{\sqrt{2}} \text{ (unstable)}, (v, q, \chi) \in \mathcal{M}_0^\pm \right\}. \quad (2.8)$$

Here \mathcal{U}^\pm is a compact interval containing ± 1 and not containing ∓ 1 .

The main technical result of [39, Chapter 3] is that $W^{u/s}(\mathcal{M}_0^\pm)$ C^3 -smoothly perturb for $0 < \varepsilon \ll 1$ to $W_\varepsilon^{u/s,\pm}$. Their transversal intersection defines $\mathcal{M}_\varepsilon^\pm := W_\varepsilon^{u,\pm} \cap W_\varepsilon^{s,\pm}$, which is a C^3 -smooth perturbation of \mathcal{M}_0^\pm . Moreover, $W_\varepsilon^{u/s,\pm}$ are locally invariant unstable and stable manifolds of $\mathcal{M}_\varepsilon^\pm$ in the sense of Fenichel – that is, orbits in $W_\varepsilon^{u,\pm}$ approach $\mathcal{M}_\varepsilon^\pm$ backwards in x with exponential rate, and orbits in $W_\varepsilon^{s,\pm}$ approach $\mathcal{M}_\varepsilon^\pm$ forwards in x with exponential rate. The proof of this result follows the steps taken in [15], in particular using the Hadamard graph transform, where uniform estimates obtained therein from the compactness of the underlying critical manifold are replaced by uniform estimates on the vector field (2.3). The proof of smoothness in ε (see [39, Chapter 3] for full details) follows the approach of [13], in particular Theorem 6 therein. These persistence results provide us with the existence of a function $u^\pm(v, q, \chi; \varepsilon) = \pm 1 + \mathcal{O}(\varepsilon)$ parametrising the u -component of $\mathcal{M}_\varepsilon^\pm$ as a graph over (v, q, χ) , which can be used to study the slow dynamics on $\mathcal{M}_\varepsilon^\pm$, given by

$$\begin{aligned} v_x &= q, \\ q_x &= (1 + f_1(\chi))v - (1 + f_2(\chi))u^\pm(v, q, \chi; \varepsilon), \\ \chi_x &= 1. \end{aligned}$$

The results on nonlinear exponential dichotomies by Fenichel [16] can now be used to prove that the slow stable and unstable manifolds $W_{slow}^{u/s}(\text{BO}_0^\pm)$ perturb C_1 -smoothly (w.r.t. the dynamics (2.9)), and that their transversal intersection $\text{BO}_{\varepsilon,R}^\pm$ is a C_1 -smooth perturbation of the reduced singular bounded orbit $\text{BO}_{0,R}^\pm$. In addition, the (perturbed) manifolds $W_{slow}^u(\text{BO}_\varepsilon^\pm) \subseteq \mathcal{M}_\varepsilon^\pm$ and $W_{slow}^s(\text{BO}_\varepsilon^\pm) \subseteq \mathcal{M}_\varepsilon^\pm$ are the stable and unstable manifolds of $\text{BO}_{\varepsilon,R}^\pm$ in the sense of Fenichel (w.r.t. the dynamics (2.9)). We obtain the background orbits $\text{BO}_\varepsilon^\pm$ in (2.3) as the image of $\text{BO}_{\varepsilon,R}^\pm$ under the inclusion map $\mathcal{M}_\varepsilon^\pm \hookrightarrow \mathbb{R}^5$. The resulting geometry is similar to that in the singular limit; now, the intersection of $W_{slow}^{u/s}(\text{BO}_\varepsilon^\pm)$ with the hyperplane $\{\chi = \chi_0\}$ is a Fenichel fibre $\mathcal{F}^{u/s,\pm}(\chi_0)$, see also Figure 3. The (u, v) -components of the perturbed background orbits $\text{BO}_\varepsilon^\pm$ correspond to the bounded stationary background states whose existence and properties are stated in Result 2.1.

Remark 2.5. Already foreshadowing the construction of stationary front solutions via Melnikov analysis, we want to emphasise that in the compact case it is sufficient to have that $W^{u/s}(\mathcal{M}_0^\pm)$ is a C^2 -smooth perturbation to ensure C^1 -smoothness of the Melnikov function. In the non-compact case one needs to go a step further and demand bounded C^3 -smoothness which then implies uniform C^2 -smoothness without compactness.

Remark 2.6. In [39] it is shown that the background solutions from Result 2.1 are stable, hence, making (1.1) a bi-stable PDE.

Remark 2.7. In the present equation setting the critical and slow manifold are different. This is in contrast with the corresponding system in [3] where the critical and slow manifold coincide. In that respect, the setting studied here is more representative of the general case.

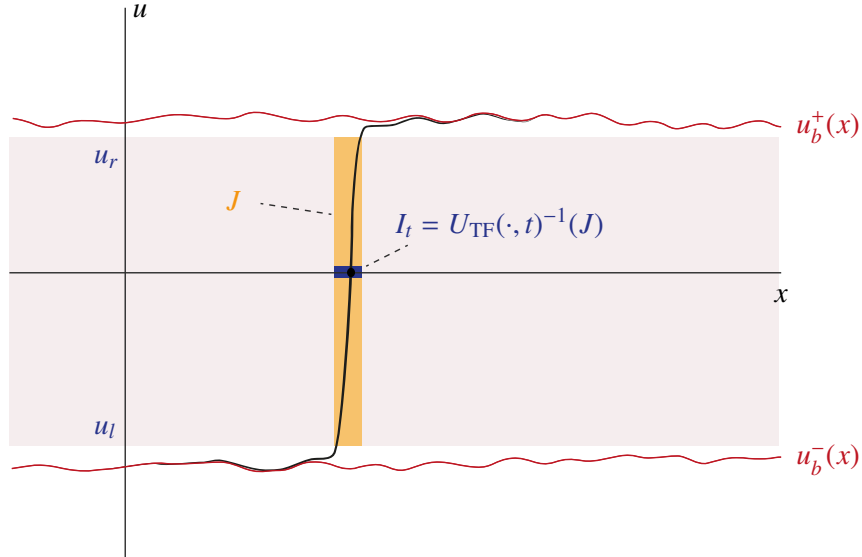


Figure 4: A visual representation of a travelling front solution as described in Definition 3.1.

3 Front solutions

While the concept of a travelling front is intuitively unambiguous, it turns out to be useful to provide a formal description of a travelling front solution to (1.1), as the presence of spatial heterogeneities introduces non-trivial spatio-temporal features to such solutions.

Definition 3.1 (Front solutions). *Let (u_b^\pm, v_b^\pm) be the stationary background states from Result 2.1. A front solution (U_F, V_F) is a bounded solution of (1.1) satisfying the following properties for all $t \in \Psi$ where either $\Psi = [t_0, \infty)$ for some $t_0 \in \mathbb{R}$ or $\Psi = \mathbb{R}$:*

1. **(Regularity)** (U_F, V_F) is C^2 -smooth in x and C^1 -smooth in t for $t \in \Psi$.
2. **(Asymptotic behaviour in space)** For every $t \in \Psi$, $(U_F(\cdot, t), V_F(\cdot, t))$ is asymptotic to the stationary background states $(u_b^\pm(x), v_b^\pm(x))$ as $x \rightarrow \pm\infty$.
3. **(Front interface properties)** There exists an interval $J := [u_l, u_r]$, $u_l < 0 < u_r$ such that for all $t \in \Psi$
 - (a) $I_t := U_F^{-1}(\cdot, t)(J)$ is an interval,
 - (b) $U_F(\cdot, t)$ is a bijection between I_t and J ,
 - (c) $0 < \inf_{t \in \Psi} |I_t|$ and $\sup_{t \in \Psi} |I_t| < \infty$, where $|I_t|$ is the length of the interval I_t .
4. **(Uniform decay in tails)** The decay of the solution at $\pm\infty$ to the background states is uniform in $t \in \Psi$.

Definition 3.2 (Entire front solutions). *We call a front solution from Definition 3.1 an entire front if $\Psi = \mathbb{R}$.*

The front interface properties described in Definition 3.1 characterise a travelling front solution by the fact that a clearly defined front connection between the two stationary background states persists for an open time interval $\Psi \subset \mathbb{R}$. In particular, properties 3a and 3b specify that, for fixed t , this front interface is a monotonically increasing graph over an x -interval I_t . Property 3c ensures that this interval persists in time, i.e. does not disappear or stretch to infinity. For a visual representation of Definition 3.1, see Figure 4. Note that Definition 3.1 confines our analysis to fronts that are left asymptotic to (u_b^-, v_b^-) and right asymptotic to (u_b^+, v_b^+) , for which the connecting front is monotonically increasing in x . This choice has been made for clarity of presentation; fronts that are left asymptotic to (u_b^+, v_b^+) and right asymptotic to (u_b^-, v_b^-) can be analysed in an analogous manner.

While in the constant-coefficient case (1.2) it is taken for granted that uniformly travelling front solutions exist for all time, a similar result for (1.1) will require considerably more effort. In particular, it will turn out to be necessary to first treat the initial value problem (leading to Definition 3.5 where Ψ from Definition 3.1 is not \mathbb{R}) to then prove the existence of entire solutions as given in Definition 3.2.

3.1 Stationary front solutions

Definition 3.1 does not specify any temporal behaviour of travelling front solutions to (1.1): in particular, stationary front solutions fall within the class of solutions described in Definition 3.1. Although the main focus of this paper is on the existence of genuinely travelling fronts, i.e. those with non-trivial temporal behaviour, it is necessary to briefly treat the existence of stationary front solutions to (1.1), as these can serve as attractors for the front solutions to (1.1) that do evolve in time.

Result 3.3 (1-parameter family of stationary fronts). *Let the conditions of Result 2.1 be fulfilled such that there exist background states (u_b^\pm, v_b^\pm) . There exists $\tilde{\varepsilon}_0 > 0$ (ε_0 from Result 2.1) and a unique C^1 -smooth function $\gamma_{SF}(x_0; \varepsilon)$ defined on $\mathbb{R} \times [0, \varepsilon_0]$ such that for $\varepsilon \in (0, \varepsilon_0]$ and $\gamma = \gamma_{SF}(x_0; \varepsilon)$ there exists a stationary front as defined in Definition 3.1 of the PDE (1.1). Its spatial profile (U_{SF}, V_{SF}) (which depends on the parameters x_0, ε) satisfies the following properties:*

1. **(Front position)** $U_{SF}(x_0; x_0, \varepsilon) = 0$.
2. **(Regularity and limiting behaviour)** *The v -component of the front $(x, x_0, \varepsilon) \rightarrow V_{SF}(x; x_0, \varepsilon)$ extends C^1 -smoothly to $\{\varepsilon = 0\}$. The u -component of the front $(x, x_0, \varepsilon) \rightarrow U_{SF}(x; x_0, \varepsilon)$ extends C^1 -smoothly to $\{\varepsilon = 0, x \neq x_0\}$ and its limit satisfies $U_{SF}(x; x_0, 0) = -1 + 2\chi_{(x_0, \infty)}(x)$.*
3. **(Leading term of existence condition)** $\gamma_{SF}(x_0; 0)$ is given by

$$\alpha v_{SF}(x_0; 0) + \gamma_{SF}(x_0; 0) = 0,$$

$v_{SF}(x_0; 0) := V_{SF}(x_0; x_0, 0)$ is given by

$$v_{SF}(x_0; 0) = \frac{2 \frac{d}{dx} v_b^-(x_0; 0) - v_b^-(x_0; 0)(a_s(x_0) + a_u(x_0))}{a_s(x_0; \cdot) - a_u(x_0)},$$

arising from the intersection of lines $\ell^{u,-}(x_0)$ and $\ell^{s,+}(x_0)$ from (2.7) that have slopes $a_{s/u}(x)$ given by unique positive, respectively negative bounded solutions of the Riccati differential equation

$$a_x = 1 + \delta_1 \tilde{f}_1(x) - a^2, \quad f_1 = \delta_1 \tilde{f}_1.$$

Furthermore, one has $\|a_u(\cdot) - 1\|_\infty = O(\delta_1)$ and $\|a_s(\cdot) + 1\|_\infty = O(\delta_1)$.

Result (3.3) is stated as a Theorem in [39, Chapter 3], where its full proof can be found. As with Result 2.1, we omit the details of that proof here, and provide a brief outline of the proof structure.

The proof of Result 3.3 uses the geometric concepts that were introduced in the proof of Result 2.1, in particular the stable and unstable manifolds $W_\varepsilon^{u/s, \pm}$ of the manifold $\mathcal{M}_\varepsilon^\pm$, which to leading order in ε are given by $W^{u/s}(\mathcal{M}_0^\pm)$ (2.8) and \mathcal{M}_0^\pm (2.5), respectively. A stationary front solution to (1.1) is a heteroclinic orbit in (2.3) that connects BO_ε^- to BO_ε^+ ; these background orbits are given to leading order in ε by BO_0^\pm (2.6).

A heteroclinic orbit from BO_ε^- to BO_ε^+ lies in the intersection $W_\varepsilon^{u,-} \cap W_\varepsilon^{s,+}$, which to leading order in ε is given by

$$W^u(\mathcal{M}_0^-) \cap W^s(\mathcal{M}_0^+) = \left\{ u \in \mathcal{U}^+ \cap \mathcal{U}^-, p = \frac{1-u^2}{\sqrt{2}}, (v, q, \chi) \in \mathcal{M}_0^\pm \right\}. \quad (3.4)$$

In the fast spatial coordinate $\xi = \frac{x}{\varepsilon}$, the relation $u_\xi = p = \frac{1-u^2}{\sqrt{2}}$ (2.3) yields the leading order front profile $\tanh \frac{\xi}{\sqrt{2}}$. The transversality and persistence in ε of the intersection (3.4) is proven in [39] by the study of the properties of a Melnikov function $M(v, q, \chi; \varepsilon)$ that measures the distance between $W_\varepsilon^{u,-}$ and $W_\varepsilon^{s,+}$, which to leading order in ε is given by

$$M(v, q, \chi; 0) = 2\sqrt{2}(\alpha v + \gamma). \quad (3.5)$$

Furthermore, the dynamics on $\mathcal{M}_\varepsilon^\pm$, which are given by (2.9), are characterised by $W_{\text{slow}}^{u/s}(\text{BO}_\varepsilon^\pm)$, see also Figure 3. To leading order in ε , we have

$$W_{\text{slow}}^{u/s}(\text{BO}_0^\pm) = \left\{ u = \pm 1, p = 0, q = \frac{dv_b^\pm}{dx}(\chi; 0) + a_{u/s}(\chi) (v - v_b^\pm(\chi; 0)) \right\},$$

where $a_{u/s}$ are the slopes of the unstable/stable lines corresponding to the exponential dichotomy of the homogeneous equation $v_{xx} = (1 + f_1(\chi))v$. As the stationary front described in Result 3.3 lies in the intersection $W^u(\text{BO}_\varepsilon^-) \cap W^s(\text{BO}_\varepsilon^+)$, we can track their intersection through $W_{\text{slow}}^u(\text{BO}_\varepsilon^-)$ via the fast transition $W_\varepsilon^{u,-} \cap W_\varepsilon^{s,+}$ to $W_{\text{slow}}^s(\text{BO}_\varepsilon^+)$. This yields, to leading order in ε , the existence condition

$$\frac{dv_b^-}{dx}(\chi; 0) + a_u(\chi)(v - v_b^-(\chi; 0)) = \frac{dv_b^+}{dx}(\chi; 0) + a_s(\chi)(v - v_b^+(\chi; 0)),$$

which can be solved for v to give

$$v_{\text{SF}} = \frac{1}{a_s(\chi) - a_u(\chi)} \left(\frac{dv_b^-}{dx}(\chi; 0) - \frac{dv_b^+}{dx}(\chi; 0) + a_s(\chi)v_b^+(\chi; 0) - a_u(\chi)v_b^-(\chi; 0) \right),$$

which together with the leading order Melnikov condition $M(v, q, \chi; 0) = 0$ (3.5) yields existence condition (3.1).

Remark 3.4. For $f_1 = f_2 = 0$ the leading order existence condition (3.1) reduces to (1.3). Moreover, if $f_1 = 0$ and f_2 is non-zero fulfilling Assumption 1.1 then the existence (3.1) is given by $\alpha \frac{d}{dx} v_b^-(x_0; 0) + \gamma_{\text{SF}}(x_0; 0) = 0$. Note that these conditions reflect, in particular, the loss of translation-invariance in space, that is, while in the constant coefficient case the fronts come in families parametrised by an arbitrary position, in the heterogeneous case only specific positions x_0 are selected.

3.2 Travelling fronts with non-zero speed

We now move to travelling front solutions with non-zero speed. We will formulate all results for the special case $f_1 = 0$. Similarly as for stationary fronts, the case $f_1 \neq 0$ is only more technical but does not need new techniques. A first step in the construction of travelling entire fronts is a solid command of the initial value problem for travelling fronts. Since this is of interest in its own right, we give a separate definition of *initialised fronts*.

Definition 3.5 (Initialised front solutions). *We call a front solution (U_F, V_F) from Definition 3.1 with initial condition $(U_F, V_F)(x, t_0) = (U_0, V_0)(x)$ for some $t_0 \in \mathbb{R}$ an initialised front if $\Psi = [t_0, \infty)$.*

3.2.1 Initialised travelling fronts

We now set out to construct front solutions as in Definition 3.1 with a non-uniformly moving interface connecting *motionless* background states. We will work with the fast-reaction scaling (1.4) which is equivalent to (1.1). The key observation is that, if such solutions exist then for every fixed $s \geq s_0$ their time derivatives satisfy $(U_s, V_s)(x, s) \rightarrow 0, x \rightarrow \pm\infty$. So, instead of working directly with the solutions (U, V) we instead will study the time evolution of the time derivatives (U_s, V_s) . For sufficiently smooth functions $(U_0, V_0) = (U_0, V_0)(x)$, we define their generalised ‘time derivative’ operators through the right-hand side of the vector field of (1.4) as follows:

$$U_0^{(1)}(U_0, V_0) := \frac{1}{\varepsilon^2} \left[\varepsilon^2 \partial_x^2 U_0 + U_0 - U_0^3 - \varepsilon(\alpha V_0 + \gamma) \right],$$

$$V_0^{(1)}(U_0, V_0) := \frac{1}{\tau} \left[\partial_x^2 V_0 - V_0 + (1 + f_2(x))U_0 \right].$$

Note that, if $(U, V) = (U, V)(x, s)$ is a solution of (1.4) with $(U, V)(x, s_0) = (U_0, V_0)(x)$ then trivially $(\partial_s U, \partial_s V)(x, s_0) = (U_0^{(1)}(U_0, V_0), V_0^{(1)}(U_0, V_0))(x, s_0)$. We will often suppress the arguments (U_0, V_0) in the following for brevity and simply write $U_0^{(1)}$ and $V_0^{(1)}$.

Fronts sets Γ Next, we introduce the vector of positive bounds $\theta = (\theta_1, \theta_2)$ with $\theta_1 := (\bar{u}, \bar{v}, u_\ell, u_r)$, $\theta_2 := (m_+, m_-, n_+, n_-)$. Here \bar{u} and \bar{v} are a-priori-bounds on the solution (details in [39, Chapter 4]) and $-1 < u_\ell < 0 < u_r < 1$. We introduce the set $\Gamma^\rightarrow(\theta)$ consisting of functions $(U_0, V_0) = (U_0, V_0)(x)$ with the following properties:

1. $U_0 \in C^{4+\ell}(\mathbb{R})$, $V_0 \in C^{4+\ell}(\mathbb{R})$, $\ell \in (0, 1)$,
2. $|U_0(\cdot)| \leq \bar{u}$, $|V_0(\cdot)| \leq \bar{v}$,
3. $\lim_{x \rightarrow \pm\infty} (U_0^{(1)}(U_0, V_0)(x), V_0^{(1)}(U_0, V_0)(x)) = (0, 0)$,
4. The interval $J := (u_\ell, u_r)$ contains $\left[-\frac{1}{\sqrt{3}}, \frac{1}{\sqrt{3}}\right]$ and $I := U_0^{-1}(J)$ is a finite interval,
5. $\partial_x U_0(x) > 0$ for all $x \in I$,
6. $\lim_{x \rightarrow \pm\infty} |U_0(x) - u_b^\pm(x)| = 0$ and $\lim_{x \rightarrow \pm\infty} |V_0(x) - v_b^\pm(x)| = 0$,
7. $\left| \min_{x \in \mathbb{R}} \{U_0^{(1)}(U_0, V_0)(x), 0\} \right| \leq \frac{1}{\varepsilon} m_-$ and $\left| \max_{x \in \mathbb{R}} \{U_0^{(1)}(U_0, V_0)(x), 0\} \right| \leq \varepsilon m_+$,
8. $\left| \min_{x \in \mathbb{R}} \{V_0^{(1)}(U_0, V_0)(x), 0\} \right| \leq n_-$ and $\left| \max_{x \in \mathbb{R}} \{V_0^{(1)}(U_0, V_0)(x), 0\} \right| \leq \varepsilon n_+$,
9. $U_0^{(1)}(U_0, V_0)(x) < 0$ for $x \in I$.

Likewise we define $\Gamma^\leftarrow(\theta)$, interchanging the role of m^\pm and n^\pm in items 7 (e.g. using $m_- \varepsilon$ and $\frac{m_+}{\varepsilon}$ in 7.) and 8, and requiring $U_0^{(1)}(U_0, V_0)(x) < 0$ for $x \in I$ in 9. The sets $\Gamma^\rightarrow(\theta)$ and $\Gamma^\leftarrow(\theta)$ contain sufficiently smooth bounded function pairs $(U_0(x), V_0(x))$ that are bi-asymptotic to the background states (u_b^\pm, v_b^\pm) . The high regularity in 1 is to ensure that the time derivatives (U_s, V_s) of the PDE solution (U, V) are themselves (classical) solutions of the PDE 3.7 (shown below). Furthermore, functions in $\Gamma^\rightarrow(\theta)$ and $\Gamma^\leftarrow(\theta)$ can be characterised as fronts through the front interface properties stated in Definition 3.1. Their implicitly defined ‘time derivative’ $(U_0^{(1)}, V_0^{(1)})$ through the vector field of the system of evolution equations (1.1) converges to zero as $x \rightarrow \pm\infty$ and obeys some explicitly ε -dependent bounds that are reminiscent of the scaling relations for conventional uniformly travelling fronts, in contrast to the scaling relation between derivatives for parabolic equations. Note that the choice of J to contain $\pm\frac{1}{\sqrt{3}}$ (front property 4) is mainly technical, and to some extent arbitrary: the factor $\frac{1}{\sqrt{3}}$ is used in estimates on the size of the difference $|u_r - u_\ell|$.

One can show that there exist θ such that the union of the sets $\Gamma^\rightarrow(\theta)$ and $\Gamma^\leftarrow(\theta)$ along with stationary fronts (discussed in Result 3.3) is nonempty for $0 < \varepsilon \ll 1$. We will briefly discuss the geometric construction for cooking up elements in the proof sketch for Result 3.9 (using auxiliary compactly supported function Λ). More details can be found in [39, Chapter 4].

Temporal evolution of $(\partial_s U, \partial_s V)$. As alluded to, it will turn out to be useful to consider the linear PDE system that governs the dynamics of $\partial_s U$ and $\partial_s V$, given by

$$\begin{cases} \varepsilon^2 \partial_s (\partial_s U) = \varepsilon^2 \partial_x^2 (\partial_s U) + (1 - 3U^2) \partial_s U - \varepsilon \alpha \partial_s V, \\ \hat{\tau} \partial_s (\partial_s V) = \partial_x^2 (\partial_s V) - \partial_s V + (1 + f_2(x)) \partial_s U. \end{cases} \quad (3.7)$$

System (3.7) can be used to determine the signs of $\partial_s^2 U$ and $\partial_s^2 V$ using similar arguments as in earlier steps of the proof. A crucial part is writing $\partial_s U$ as the sum of three parts: a ‘fade out’ part, which decreases exponentially in time; an ‘interface’ part, whose properties are determined by the shape of the front interface, and a ‘tails’ part, whose properties are determined by the asymptotic convergence to the background states. For all three parts, the variation of constants formula applied to (3.7) is used to establish estimates on $|\partial_s U|$.

Positive feedback $\alpha < 0$ The aforementioned generic regularity results form the basis for the next step of the proof. When $\alpha < 0$, the set of functions (U_0, V_0) obeying properties 1, 2, 3, 6 and the additional property

$$10. \quad u_b^-(x) \leq U_0(x) \leq u_b^+(x) \text{ and } v_b^-(x) \leq V_0(x) \leq v_b^+(x)$$

can be shown to be forward invariant under the flow of (1.1), using integral estimates combined with repeatedly extending the length of finite time interval on which the results are shown to hold. In the next step, the front properties 4 and 5 are incorporated, together with the propagation direction property

$$11. \quad U_0^{(1)}(x, 0), V_0^{(1)}(x, 0) \leq 0 \text{ for all } x \in \mathbb{R} \text{ and } U_0^{(1)}(x, 0), V_0^{(1)}(x, 0) < 0 \text{ for } x \in I = U_0^{-1}([u_\ell, u_r]).$$

It can be shown that these properties are forward invariant under the flow of (1.1).

Mixed feedback $\alpha > 0$ When $\alpha > 0$, the feedback of V on U in (1.1) is negative, while the feedback of U on V remains positive. This mixed feedback has profound impact on the dynamics of travelling fronts in (1.1). Indeed, when $\alpha > 0$, the propagation direction of the front might reverse; see also Example 2 in section 4.3. A related phenomenon is that, for $\alpha > 0$, the U -component might overshoot the background states u_b^\pm , in contrast to the travelling front described in Results 4.1 and 3.10.

We will now set out to formulate an existence result for $\alpha > 0$ for front solutions that travel in one fixed direction. We formulate two results on the existence of initialised travelling fronts in the absence of stationary fronts. The results are formulated for right-travelling fronts for clarity of presentation; results on left-travelling front can be obtained in an analogous manner.

Result 3.6. *Let $\alpha > 0$ and $\sup_{x \in \mathbb{R}} \frac{dv_b^-}{dx}(x; 0) < \frac{\gamma}{\alpha}$. Fix $\theta_1 = (\bar{u}, \bar{v}, u_\ell, u_r)$, and $\theta_2 = (m_+, m_-, n_+, n_-) \in \mathbb{R}_{>0}^4$. Then there exists $\widehat{\theta}_2$ and $\varepsilon_0 > 0$ such that for all $\varepsilon \in (0, \varepsilon_0)$ and all initial conditions $(U_0, V_0) \in \Gamma^\rightarrow(\theta_1, \theta_2)$ such that $U_0(z_0) = 0$ and $U_0^{(1)}$ fulfils the condition*

$$\begin{aligned} & \text{there exist } \varkappa, \lambda_0, \underline{d} > 0 \text{ such that } \text{supp } U^{(1)}(U_0, V_0) \subset [z_0 - \varepsilon \varkappa, z_0 + \varepsilon \varkappa] \\ & \text{and } U_0^{(1)} \leq \frac{\lambda_0}{\varepsilon} \text{ for } x \in \left[U_0^{-1}(-1/\sqrt{3}) - \varepsilon \underline{d}, U_0^{-1}(1/\sqrt{3}) + \varepsilon \underline{d} \right], \end{aligned}$$

we have for the solution (U, V) of the corresponding initial value problem for (1.1) that

$$(U(\cdot, s), V(\cdot, s)) \in \Gamma^\rightarrow(\theta_1, \widehat{\theta}_2) \quad \text{for all } s > s_0.$$

This result states that the front shape of initial conditions is quantitatively preserved by the PDE flow, but not necessarily qualitatively, since the $\Gamma^\rightarrow(\theta)$ is not forward invariant.

Remark 3.7. In case the assumptions on the initial conditions are relaxed from having compact support to being sufficiently localised in space, a similar result can be formulated with the addition that the front will be formed after a short initial calibration phase that is of order $\mathcal{O}(\varepsilon^2)$ in s (or equivalently order $\mathcal{O}(1)$ in t).

Proof strategy for mixed feedback $\alpha > 0$ [39, Chapter 4] When $\alpha > 0$, both boundedness between the background states (property 3.2.1) and uniform direction of propagation (property 3.2.1) are, in contrast to the positive feedback case, not forward invariant under the flow of (1.1). As a result, crucial building blocks that were used in the proof of Results 3.9 and 3.10 are missing.

However, the existence of an initialised travelling front – i.e. a solution that maintains its front shape and has a uniform propagation direction for all $s > s_0$ – can for $\alpha > 0$ be shown using estimates on $\partial_s U$ based on the variation of constants formula applied to (3.7). The assumption $\sup_{x \in \mathbb{R}} \frac{dv_b^-}{dx}(x; 0) < \frac{\gamma}{\alpha}$ is crucial, implying that the integral $\int_{z(s)-\sqrt{\varepsilon}}^{z(s)+\sqrt{\varepsilon}} \partial_s U(x, s) dx$ is negative and uniformly bounded away from zero. Next, $\partial_s U$ is again written as the sum of three parts: a ‘fade out’ part, which decreases exponentially in time; an ‘interface’ part, whose properties are determined by the shape of the front interface, and a ‘tails’ part, whose properties are determined by the asymptotic convergence to the background states. The assumption of compact support (Result 3.6) or the assumption of initial calibration (Result 3.7) can now be used to estimate the integral of $\partial_s U$ in an ε -neighbourhood around the front position $z(s)$. Together with estimates on the ‘fade out’ part and the ‘tails’ part of $\partial_s U$, this provides a bound of the form $\partial_s U < -\frac{\lambda}{\varepsilon}$ for some $\lambda > 0$ for finite s . Next, the uniformity of the obtained estimates can be used to extend the s -interval of existence to all $s \geq s_0$, thereby proving the existence of initialised travelling front solutions to (1.4).

3.2.2 Entire travelling front solutions

To make statements about the properties of travelling fronts with nonzero speed, it is necessary to define what we mean by “position”:

Definition 3.8. *The position of an entire travelling front (U_{TF}, V_{TF}) is defined as the unique function $z(s)$ for which $U_{TF}(z(s), s) = 0$ for all $s \in \mathbb{R}$.*

The existence and uniqueness of $z(s)$ follow from the front properties stated in Definition 3.1. For stationary fronts, we have $z(s) \equiv x_0$, cf. Result 3.3. If no stationary front exists, the existence of uniformly travelling fronts is summarised in the following Result:

Result 3.9 (Entire travelling fronts). *Let $\alpha \neq 0$, $f_1 = 0$ and let f_2 satisfy Assumption 1.1.*

1. *Let $\sup_{x \in \mathbb{R}} \alpha \frac{dv_b^-}{dx}(x; 0) < \gamma$. Then there exists an $\varepsilon_0 > 0$ such that for all $0 < \varepsilon \leq \varepsilon_0$, there exists an entire travelling front. Its position satisfies $\frac{dz}{ds} > 0$; moreover, $z(s) \rightarrow \pm\infty$ as $s \rightarrow \pm\infty$, and $\left\| \frac{dz}{ds} \right\|_\infty = O(1)$ in ε .*
2. *Let $\inf_{x \in \mathbb{R}} \alpha \frac{dv_b^-}{dx}(x; 0) > \gamma$. Then there exists an $\varepsilon_0 > 0$ such that for all $0 < \varepsilon \leq \varepsilon_0$, there exists an entire travelling front. Its position satisfies $\frac{dz}{ds} < 0$; moreover, $z(s) \rightarrow \mp\infty$ as $s \rightarrow \pm\infty$, and $\left\| \frac{dz}{ds} \right\|_\infty = O(1)$ in ε .*

We refrain from giving a full proof, which can be found in [39].

Sketch of the proof for Result 3.9 We fix a non-negative compactly supported smooth even function Λ . The support (more precisely the complement of the zero level set) of Λ is an interval centred around 0, and its width is chosen such that it contains $u_h^{-1}([-\frac{1}{\sqrt{3}}, \frac{1}{\sqrt{3}}])$, where u_h is the Allen-Cahn front $u_h(\xi) = \tanh(\frac{1}{2}\sqrt{2}\xi)$. Given $z_0 \in \mathbb{R}$, we construct an initial condition (U_0, V_0) at position z_0 by enforcing that for some scalar $c \in \mathbb{R}$ the following relation holds

$$(U_0^{(1)}, V_0^{(1)})(x) = -c\Lambda\left(\frac{x - z_0}{\varepsilon}\right)(U_0'(x), V_0'(x)).$$

One can think of (3.8) as corresponding to a mixture of using a co-moving frame $\xi = \frac{x-(z_0+c(s-s_0))}{\epsilon}$ near the interface and resting frame $\xi = \frac{x-z_0}{\epsilon}$ in the tails. The interface is cut off using the function Λ . The construction is instantaneous, in the sense that the position z_0 and the speed c are fixed. Hence, we are interested in the 'germ' of stationary solutions of the PDE (1.1) in terms of the (mixed co-moving/resting) coordinates (ξ, s) , i.e. when s is infinitesimally close to s_0 , which gives (3.8). More details can be found in [39, Chapter 4].

Substituting (3.8) into the PDE gives rise to a system of nonautonomous ODEs. In the system of ODEs $z_0 \in \mathbb{R}$ appears as a parameter, and the aim is to find $\epsilon_0 > 0$ and a function $c = c(z_0, \epsilon)$ (extending smoothly to $\epsilon = 0$), such that for $c = c(z_0, \epsilon)$ and $\epsilon \in (0, \epsilon_0)$ the system of ODEs has an (appropriately defined) heteroclinic orbit. In this sense the construction parallels the construction of stationary fronts, where $c = c(z_0, \epsilon)$ takes the role of $\gamma = \gamma_{SF}(z_0, \epsilon)$ (see Result 3.3). However, a new technical challenge in the present case (which did not appear in the construction of stationary fronts) is that the system of ODEs is not a slow/fast system, due to the term $\Lambda(\frac{x-\xi}{\epsilon})$, which either makes the vector field discontinuous at $\epsilon = 0$ or forces to introduce a variable ζ which in the fast scale satisfies $\zeta_\xi = 1$ (in particular ζ is neither a fast nor a slow variable). Nevertheless, by making suitable adjustments to the (slow/fast) approach for stationary fronts, we can prove the existence of $\epsilon_0 > 0$ and the function $c(z_0, \epsilon)$ defined for $(z_0, \epsilon) \in \mathbb{R} \times [0, \epsilon_0]$.

For purposes of illustration, consider mixed feedback $\alpha > 0$ and γ as in part 1 of Result 3.9 (i.e. the case of fronts moving with positive non-zero speed). The assumptions on Λ and boundedness of the function $c(z_0, \epsilon)$ implies that the resulting initial conditions $x \rightarrow (U_0, V_0)(x; z_0, \epsilon)$ (extracted from the ODE heteroclinics) are elements of $\Gamma^\rightarrow(\theta)$. It can be shown that in fact the m^+ and n^+ components of θ are zero and that the assumptions for Result 3.6 hold (in particular $U_0^{(1)}$ has compact support by construction). Hence by Result 3.6 (for mixed feedback) there exist $\widehat{\theta}$ such that the solution $(U, V)(x, s; s_0, z_0, \epsilon)$ of the IVP with initial condition $(U_0, V_0)(x; z_0, \epsilon)$ at time s_0 satisfies $(U, V)(x, s; s_0, z_0, \epsilon) \in \Gamma^\rightarrow(\widehat{\theta})$ for all $s \geq s_0$, which includes a uniform bound on the gradient of (U, V) . In addition, it can also be seen that the decay in the tails is uniform for all $s \geq s_0$, $s_0 \in \mathbb{R}$ and $z_0 \in \mathbb{R}$. The entire solution $(U, V)_{TF}$, is extracted from the family $\{(U, V)(x, s; s_0, z_0, \epsilon) : s_0 \in \mathbb{R}, z_0 \in \mathbb{R}\}$ using the Arzelà-Ascoli theorem along with the uniform estimates for (U, V) , where the uniformity for the length of the interface and the decay in the tails helps to deal with the lack of compactness of the domain $(x, s) \in \mathbb{R}^2$.

Stationary fronts as attractor of travelling fronts for $\alpha < 0$. For $\alpha < 0$ (positive feedback) one can establish that, if stationary fronts do exist, they act as attractors for travelling front in forward and backward time, as summarised in the following Result. Its proof can be found in [39, Chapter 4], where it is seen to follow naturally from the Theorem corresponding to Result 3.9.

Result 3.10. *Let $\alpha < 0$, $f_1 = 0$, and let f_2 satisfy Assumptions 1.1. Let (U_{SF}, V_{SF}) be a stationary front with location x_0 , such that $\frac{d^2 v_b^-}{dx^2}(x_0; 0) \neq 0$.*

1. *Suppose that $\frac{d^2 v_b^-}{dx^2}(x_0; 0) > 0$. Then there exists an $\epsilon_0 > 0$ such that for all $0 < \epsilon \leq \epsilon_0$ there exists a pair of entire travelling fronts $(U_{TF}^{\leftarrow/\rightarrow}, V_{TF}^{\leftarrow/\rightarrow})$ for which $\lim_{s \rightarrow -\infty} (U_{TF}^{\leftarrow/\rightarrow}, V_{TF}^{\leftarrow/\rightarrow}) = (U_{SF}, V_{SF})$. The front velocities satisfy $\frac{dz^-}{ds} < 0$ and $\frac{dz^+}{ds} > 0$; moreover, we have $u_b^-(x) \leq U_{TF}^\rightarrow(x, s) < U_{SF}(x) < U_{TF}^\leftarrow(x, s) \leq u_b^+(x)$ and $v_b^-(x) \leq V_{TF}^\rightarrow(x, s) < V_{SF}(x) < V_{TF}^\leftarrow(x, s) \leq v_b^+(x)$.*
2. *Suppose that $\frac{d^2 v_b^-}{dx^2}(x_0; 0) < 0$. Then there exists an $\epsilon_0 > 0$ such that for all $0 < \epsilon \leq \epsilon_0$ there exists a pair of entire travelling fronts $(U_{TF}^{\leftarrow/\rightarrow}, V_{TF}^{\leftarrow/\rightarrow})$ for which $\lim_{s \rightarrow \infty} (U_{TF}^{\leftarrow/\rightarrow}, V_{TF}^{\leftarrow/\rightarrow}) = (U_{SF}, V_{SF})$. The front*

velocities satisfy $\frac{dz^{\leftarrow}}{ds} < 0$ and $\frac{dz^{\rightarrow}}{ds} > 0$; moreover, we have $u_b^-(x) \leq U_{\text{TF}}^-(x, s) < U_{\text{SF}}(x) < U_{\text{TF}}^+(x, s) \leq u_b^+(x)$ and $v_b^-(x) \leq V_{\text{TF}}^-(x, s) < V_{\text{SF}}(x) < V_{\text{TF}}^+(x, s) \leq v_b^+(x)$.

4 Delay-differential equation for front position dynamics

The results of the previous section provide general properties of the front position $z = z(s)$ from Definition 3.8. In order to study the dynamics of $z(s)$ in more detail, one can derive an evolution equation for the front position. The outcome of this analysis, as carried out in [39, Chapter 5], is formulated in the following Result:

Result 4.1 (Delay-differential equation). *Let $f_1 = 0, \varepsilon_0 > 0$ and let $(U_{TF}(x, s; \varepsilon), V_{TF}(x, s; \varepsilon))$ be a family of entire travelling front solutions (as given in Results 3.9) parametrised by $\varepsilon \in (0, \varepsilon_0)$, with front position $z(s; \varepsilon)$. The singular limit $z_R(s) := \lim_{\varepsilon \downarrow 0} z(s; \varepsilon)$ obeys the equation*

$$\frac{\sqrt{2}}{3} \frac{dz_R}{ds} = \gamma + \alpha \left(\frac{dv_b^+}{dx}(z_R(s); 0) + \hat{\tau} W[z_R](s) \right), \quad (4.1)$$

where $W[z]$ is the functional

$$W[z](s) := \frac{1}{2\sqrt{\pi\hat{\tau}}} \int_{-\infty}^s \int_{-\infty}^0 \frac{dz}{ds}(r) (1 + f_2(z(r))) \frac{1}{\sqrt{s-r}} e^{x+\frac{r-s}{\hat{\tau}}} \left[e^{-\frac{\hat{\tau}}{4(s-r)}(x-(z(s)-z(r)))^2} + e^{-\frac{\hat{\tau}}{4(s-r)}(x+(z(s)-z(r)))^2} \right] dx dr. \quad (4.2)$$

Equation (4.1) is derived rigorously in [39, Chapter 5] in the case $\alpha < 0$, for which the existence of the ε -family of entire front solutions is provided by Results 3.9 and 3.10. For general α , assuming the existence of a ε -family of front solutions, equation (4.1) can be formally derived using the approach sketched below. Numerical simulations suggest that (4.1) indeed also holds for $\alpha > 0$.

Remark 4.2. An implicit version of the above delay-differential equation is given by

$$\begin{aligned} \alpha V_R(z_R(s), s) + \gamma &= \frac{\sqrt{2}}{3} z'_R(s), \\ \hat{\tau} \partial_s V_R &= \partial_x^2 V_R - V_R + (1 + f_2(x)) \text{sign}(x - z_R(s)). \end{aligned}$$

In [3] a coupled algebraic-ODE system was formally derived to describe the dynamic position of travelling pulse solutions that bifurcated through a drift instability from a stationary one. Here we get for $\hat{\tau} > 0$ a PDE which boils down to an ODE for $\hat{\tau} = 0$.

4.1 Formal derivation

Before showing the formal derivation, we provide a short overview. To derive (4.1), we mimic the approach for stationary fronts from Section 3.1, writing (1.1) as a "time-dependent spatial dynamics system" (with U_{TF}, V_{TF} as in Result 4.1)

$$\begin{aligned} \varepsilon u_x &= p, \\ \varepsilon p_x &= -u + u^3 + \varepsilon(\alpha v + \gamma) + \varepsilon^2 \partial_s U_{TF}(x, s; \varepsilon), \\ v_x &= q, \\ q_x &= v - (1 + f_2(x))u + \hat{\tau} \partial_s V_{TF}(x, s; \varepsilon). \end{aligned}$$

We are interested in the singular limit $\varepsilon = 0$, which gives, with z_R as in Result 4.1

$$\begin{aligned} v_x &= q, \\ q_x &= v - (1 + f_2(x))\text{sign}(x - z_R(s)) + \hat{\tau}\partial_s V_R(x, s). \end{aligned}$$

Treating $\hat{\tau}\partial_s V_R$ as an inhomogeneity of the (v, q) -system, we find (cf. (2.1)) to leading order

$$V_R(x, s) = \begin{cases} v_b^-(x; 0) - G(\hat{\tau}\partial_s V_R(\cdot, s)) - (v_b^-(z_R(s); 0) + \frac{dv_b^-}{dx}(z_R(s); 0))e^{x-z_R(s)} & \text{for } x < z_R(s) \\ v_b^+(x; 0) - G(\hat{\tau}\partial_s V_R(\cdot, s)) - (v_b^+(z_R(s); 0) + \frac{dv_b^+}{dx}(z_R(s); 0))e^{-x+z_R(s)} & \text{for } x > z_R(s) \end{cases}$$

Taking the partial derivative w.r.t. s and equating $\partial_s v_R(x, s) = \partial_s V_R(x, s)$ yields the following PDE for $w(x, s) := -G(\partial_s V_R(\cdot, s))$:

$$\hat{\tau}\partial_s w = \partial_x^2 w - w + z_R'(s)(1 + f_2(z_R(s)))e^{-|x-z_R(s)|} \quad (4.5)$$

By analogy with the constant coefficient case $f_2 = 0$ it seems plausible that to leading order in ε the following Melnikov condition should hold

$$\frac{\sqrt{2}}{3} \frac{dz_R}{ds} = \alpha V_R(z_R(s), s) + \gamma.$$

Using the explicit form of the heat semigroup on (4.5) yields Result 4.1.

We will discuss the formal derivation in more detail. For convenience, we drop the index R in the notation V_R and z_R , which will not result in confusion as this section involves only the singular limit $\varepsilon = 0$. We will also use the notation $q_b^\pm := \frac{dv_b^\pm}{dx}$

Preliminaries The starting point is to borrow intuition from the constant coefficient case when $f_2 = 0$. In that case, there exist for $0 < \varepsilon \ll 1$ travelling fronts which travel with constant speed $c(\varepsilon)$, which in the singular limit $\varepsilon \downarrow 0$ satisfies (1.3), which we recall here for clarity

$$\alpha v^*(c) + \gamma = \frac{\sqrt{2}}{3} c, \quad v^*(c) = \frac{\hat{\tau}c}{\sqrt{4 + c^2 \hat{\tau}^2}}$$

where $v^*(c)$ is the value of V at the interface of the step function $U = \text{sign}(x - z(s))$, and $z(s) = z_0 + cs$ is the position of the interface at time s . By analogy, it is plausible that when the heterogeneity f_2 is introduced, the following existence condition should hold (justifying this rigorously requires much more work, in particular proving existence of travelling fronts (U, V) for $0 < \varepsilon \ll 1$ and studying the limit behaviour (U, V) as well as the gradient (U_x, U_s, V_x, V_s) as $\varepsilon \downarrow 0$, and is one of the main topics of [39].)

$$\alpha V(z(s), s) + \gamma = \frac{\sqrt{2}}{3} z'(s).$$

To compute $V(z(s), s)$ we note that $V(x, s)$ should be a front solution of the inhomogeneous scalar PDE

$$\hat{\tau}V_s = V_{xx} - V + (1 + f_2(x))\text{sign}(x - z(s)) \quad (4.8)$$

where the inhomogeneity has a discontinuity at $x = z(s)$. The first intuition would be to write down the variation of constants formula

$$V(x, s) := \int_{-\infty}^s \int_{-\infty}^{\infty} \frac{1}{\hat{\tau}} (1 + f_2(x - y)) \text{sign}(x - y - z(u)) \frac{\sqrt{\hat{\tau}}}{\sqrt{4\pi} \sqrt{s - u}} \exp\left(-\frac{y^2 \hat{\tau}}{4(s - u)}\right) \exp\left(-\frac{s - u}{\hat{\tau}}\right) dy du,$$

however, it turns out to be difficult to distil a meaningful expression for $V(z(s), s)$ in a direct way (i.e. by manipulating the integrals using change of variables, partial integration etc).

GSPT approach to the time-dependent spatial dynamics system (4.3) We will look from a geometric point at the situation and derive a relation (see (4.13)) between $V(z(s), s)$ and $G(V_s(\cdot, s))(z(s))$, where (see Result 2.1)

$$G(f)(x) := -\frac{1}{2} \left(\int_x^{\infty} e^{-y} f(y) dy \right) e^x - \frac{1}{2} \left(\int_{-\infty}^x e^y f(y) dy \right) e^{-x}.$$

is the solution operator corresponding to the ODE $v'' - v = f$. To this end we consider for fixed $s \in \mathbb{R}$ the reduced slow systems given by

$$\begin{aligned} v' &= q \\ q' &= v - (1 + f_2(x))u + \hat{\tau}V_s(x, s), \\ u &\in \{-1, 1\} \end{aligned} \tag{4.9}$$

where we view $V_s(\cdot, s)$ as an inhomogeneity (and for the moment ignoring the relation between V_s and V). If the term $V_s(x, s)$ would not be present, then (under assumptions A1 and A2 on f_2) the system (4.9) with $u = -1$ has a unique bounded negative solution (i.e. singular limit background state) $(v_b^-, q_b^-)(x, 0)$, $x \in \mathbb{R}$ and a unique bounded positive solution $(v_b^+, q_b^+)(x, 0)$, $x \in \mathbb{R}$. The solution V of (4.8) which we would like to construct satisfy the following properties.

1. (connect negative background state in backward time) $\{(V(x, s), V_x(x, s)), x \leq z(s)\}$ which is a (backward) orbit of (4.9) for $u = -1$, should connect to $(v_b^-, q_b^-)(x, 0)$ as $x \rightarrow -\infty$.
2. (connect positive background state in forward time) Likewise $\{(V(x, s), V_x(x, s)), x \geq z(s)\}$ is an orbit of (4.9) for $u = 1$ which should connect to $v_b^+(x, 0)$ as $x \rightarrow \infty$.
3. (heteroclinic) These backward and forward orbits should match at $x = z(s)$
4. (Melnikov condition) $V(z(s), s)$ should satisfy the Melnikov condition (4.7)

We will interpret the effect of the inhomogeneity $x \rightarrow V_s(x, s)$ in (4.9) as a distortion of the background states $(v_b^\pm(x; 0))$ near the interface $x = z(s)$ such that the construction described can be carried out for all $s \in \mathbb{R}$. Indeed, if the inhomogeneity $V_s(\cdot, s)$ in (4.9) would not be present, then geometrically, the conditions imply that the three lines $(v_b^-, q_b^-)(z(s); 0) + \mathbb{R}(1, 1)$ and $-(v_b^+, q_b^+)(z(s), 0) + \mathbb{R}(1, -1)$, and $\alpha v + \gamma = \frac{\sqrt{2}}{3} z'(s)$ in the (v, q) plane have to intersect for all $s \in \mathbb{R}$. This situation is very rigid, e.g. even if we consider just a single value of s , we still need three lines to intersect, which we can only expect to happen at a small number of positions $z(s) = s$. In particular setting $z'(s) = 0$ and $z(s)$ is equal to (a small number of) specific positions, leads to the construction of stationary fronts.

In view of the preceding discussion, define

$$\begin{aligned} v_{b,\text{dist}}^\pm(x; s) &:= v_b^\pm(x, 0) + \tilde{v}(x; s) \\ \tilde{v}(x; s) &:= \hat{\tau}G(V_s(\cdot, s))(x) \end{aligned} \quad (4.10)$$

here we interpret $v_{b,\text{dist}}^\pm$ as distorted background states. Note that $v_b^\pm(x, 0) = -(\pm)G(1 + f_2(x))$. Define $\tilde{q}(x; s) = \frac{d}{dx}\tilde{v}(x; s)$ and $q_{b,\text{dist}}^\pm(x; s) = \frac{d}{dx}\tilde{v}(x; s)$. The effect of the distortion is to make the following lines in the (v, q) -plane intersect

- The vertical line $\alpha v + \gamma = \frac{\sqrt{2}}{3}z'(s)$. Let

$$v^*(s) := \frac{1}{\alpha} \left(\frac{\sqrt{2}}{3}z'(s) - \gamma \right).$$

- The line

$$\left\{ (v, q) \in \mathbb{R}^2 \mid (v, q) = -(v_b^-, q_b^-)(z(s); 0) + (\tilde{v}(z(s); s), \tilde{q}(z(s); s)) + \mathbb{R}(1, 1) \right\}, \quad (4.11)$$

which if we make (4.9), $u = -1$ autonomous by setting $\chi_x = 1$, we may interpret as the unstable manifold of the distorted background state $(v_{b,\text{dist}}^-, q_{b,\text{dist}}^-)(x; s)$ viewed in the slice $\{\chi = z(s)\}$.

- The line

$$\left\{ (v, q) \in \mathbb{R}^2 \mid (v, q) = (v_b^-, q_b^-)(z(s), 0) + (\tilde{v}(z(s); s), \tilde{q}(z(s); s)) + \mathbb{R}(1, -1) \right\}, \quad (4.12)$$

which if we make (4.9), $u = +1$ autonomous by setting $\chi_x = 1$, we may interpret as the stable manifold of the distorted background state $(v_{b,\text{dist}}^+, q_{b,\text{dist}}^+)(x; s)$ viewed in the slice $\{\chi = z(s)\}$.

To see when the lines (4.11) and (4.12) intersect at $v = v^*$ we consider the following lemma.

Lemma 4.3. *Let $a, b, c, d \in \mathbb{R}$ and let ℓ_i , $i = 1, 2, 3$ be 3 lines of the form $\ell_1 : (v, q) = [(a, b) + (c, d)] + \mathbb{R}(1, 1)$, $\ell_2 : (v, q) = [-(a, b) + (c, d)] + \mathbb{R}(1, -1)$ and $\ell_3 : v = v^*$. Then ℓ_i intersect in a single point if and only if $c = v^* + b$.*

Proof: We need to solve the (overdetermined) system of equations $a + c + t = v^*$, $-a + c + s = v^*$ and $b + d + t = -b + d - s$ for s, t . From the first two equations show $t = v^* - a - c$ and $s = v^* + a - c$. Substituting in the third equations gives the compatibility condition $c = v^* + b$. ■

Applying Lemma 4.3 to (4.11) and (4.12) (and recalling $(v_b^+, q_b^+) = -(v_b^-, q_b^-)$) gives $\tilde{v}(z(s); s) = v^*(s) + q_b^-(z(s); 0)$. Recalling $\tilde{v}(z(s); s) = -\hat{\tau}G(V_s(\cdot, s))(z(s))$ (see (4.10)), and using that $V(z(s), s)$ should be equal to $v^*(s)$ we obtain the relation

$$V(z(s), s) = \tilde{v}(z(s); s) - q_b^-(z(s), 0) = -\hat{\tau}G(V_s(\cdot, s))(z(s)) - q_b^-(z(s), 0).$$

In addition we have

$$\begin{aligned} V(x, s) &= v_{b,\text{dist}}^-(x; s) + A \exp(x) \text{ if } x \leq z(s) \\ V(x, s) &= v_{b,\text{dist}}^+(x; s) + B \exp(-x) \text{ if } x \geq z(s), \end{aligned}$$

for constants A, B . Using that $v_{b,\text{dist}}^\pm(z(s); s) = v_b^\pm(z(s); 0) + V(z(s); s) + q_b^\mp(z(s); 0)$ (in view of 4.13), we obtain

$$\begin{aligned} A &= -(v_b^-(z(s); 0) + q_b^-(z(s); 0) \exp(-z(s))) \\ B &= -(v_b^+(z(s); 0) + q_b^-(z(s); 0) \exp(z(s))) \end{aligned}$$

In particular note that $q_b^-(z(s); 0)$ appears in both equations (so it is not q_b^- in one equation and q_b^+ in the other). In summary we have found

$$V(x, s) = \begin{cases} v_b^-(x; 0) - \hat{\tau}G(V_s(\cdot, s))(x) - (v_b^-(z(s); 0) + q_b^-(z(s); 0)) \exp(x - z(s)) & \text{if } x \leq z(s), \\ v_b^+(x; 0) - \hat{\tau}G(V_s(\cdot, s))(x) - (v_b^+(z(s); 0) + q_b^-(z(s); 0)) \exp(-(x - z(s))) & \text{if } x \geq z(s) \end{cases}$$

Deriving an expression for $W[z_0]$ So far we viewed s as fixed and looked at the profile $x \rightarrow V(x, s)$. We will now look at V as a function of two variables (x, s) . Set $\omega(x, s) := -G(V_s(\cdot, s))(x)$. We differentiate (4.14) w.r.t s . On the left hand side of (4.14) we get $V_s(x, s) = \omega_{xx} - \omega$.

On the right hand side we compute

$$\begin{aligned} \partial_s \left[(v_b^-(z(s); 0) + q_b^-(z(s); 0)) \exp(x - z(s)) \right] &= \\ z'(s)(q_b^-(z(s); 0) + v_b^-(z(s); 0) + (1 + f_2(z(s)))) \exp(x - z(s)) &= \\ - z'(s)(v_b^-(z(s); 0) + q_b^-(z(s); 0)) \exp(x - z(s)) &= \\ = z'(s)(1 + f_2(z(s))) \exp(x - z(s)) \end{aligned}$$

Likewise we compute using $(v_b^+, q_b^+) = -(v_b^-, q_b^-)$

$$\begin{aligned} \partial_s \left[(v_b^+(z(s); 0) + q_b^-(z(s); 0)) \exp(-(x - z(s))) \right] &= \\ z'(s)(q_b^+(z(s); 0) + v_b^+(z(s); 0) - (1 + f_2(z(s)))) \exp(-(x - z(s))) &= \\ + z'(s)(v_b^+(z(s); 0) + q_b^-(z(s); 0)) \exp(-(x - z(s))) &= \\ = z'(s)(1 + f_2(z(s))) \exp(-(x - z(s))) \end{aligned}$$

We have

$$\partial_x^2 \omega - \omega = \hat{\tau} \partial_s \omega + h(x, s),$$

where

$$h(x, s) = -z'(s)(1 + f_2(z(s))) \exp(-|x - z(s)|)$$

Applying the Fourier transform (with respect to the variable x) and rearranging

$$\hat{\tau} \partial_s \hat{\omega} + (k^2 + 1) \hat{\omega} = -\hat{h}(k, s)$$

For each fixed k this is a linear first order ODE. Denoting $\hat{\omega}_0(k) := \hat{\omega}(k, 0)$ we have

$$\hat{\omega}(k, s) = \exp\left(-\frac{k^2 + 1}{\hat{\tau}} s\right) \left[\hat{\omega}_0(k) - \int_0^s \frac{1}{\hat{\tau}} \hat{h}(k, u) \exp\left(\frac{k^2 + 1}{\hat{\tau}} u\right) du \right]$$

We determine $\hat{\omega}_0(k)$ by imposing that the solution $s \rightarrow \hat{\omega}(k, s)$ should be bounded. Assuming $\hat{\tau} > 0$ we can write

$$\hat{\omega}(k, s) = \exp\left(-\frac{k^2 + 1}{\hat{\tau}}s\right) \left[- \int_{-\infty}^s \frac{1}{\hat{\tau}} \hat{h}(k, u) \exp\left(\frac{k^2 + 1}{\hat{\tau}}u\right) du \right]$$

Using $\mathcal{F}(x \rightarrow \exp(-|x - z(u)|)) = e^{-ikz(u)} \mathcal{F}(x \rightarrow \exp(-|x|))$ we obtain

$$\hat{\omega}(k, s) = \mathcal{F}(\exp(-|\cdot|)) \int_{-\infty}^s \frac{1}{\hat{\tau}} z'(u) (1 + f_2(z(u))) \exp\left(\frac{k^2 + 1}{\hat{\tau}}(u - s) - ik(z(u))\right) du$$

We now examine the inverse Fourier transform of the integral in the second line. For $u < s$ we have

$$\frac{1}{\sqrt{2\pi}} \int_{-\infty}^{\infty} e^{ikx} \exp\left(\frac{k^2 + 1}{\hat{\tau}}(u - s) - ik(z(u))\right) dk = \frac{\sqrt{\hat{\tau}}}{\sqrt{2} \sqrt{s - u}} \exp\left(\frac{(z(u) - x)^2 \hat{\tau}}{4(u - s)}\right) \exp\left(\frac{u - s}{\hat{\tau}}\right)$$

We obtain

$$\begin{aligned} \omega(y, s) &= \frac{1}{\sqrt{2\pi}} \int_{-\infty}^s \int_{-\infty}^0 \frac{1}{\hat{\tau}} z'(u) (1 + f_2(z(u))) \frac{\sqrt{\hat{\tau}}}{\sqrt{2} \sqrt{s - u}} \exp\left(\frac{u - s}{\hat{\tau}}\right) \\ &\quad e^x \left[\exp\left(\frac{-(-y + x + z(u))^2 \hat{\tau}}{4(s - u)}\right) + \exp\left(\frac{-(-y - x + z(u))^2 \hat{\tau}}{4(s - u)}\right) \right] dx du \end{aligned}$$

In particular,

$$\begin{aligned} \omega(z(s), s) &= \frac{1}{\sqrt{2\pi}} \int_{-\infty}^s \int_{-\infty}^0 \frac{1}{\hat{\tau}} z'(u) (1 + f_2(z(u))) \frac{\sqrt{\hat{\tau}}}{\sqrt{2} \sqrt{s - u}} \exp\left(\frac{u - s}{\hat{\tau}}\right) \\ &\quad e^x \left[\exp\left(\frac{-(-x - [z(s) - z(u)])^2 \hat{\tau}}{4(s - u)}\right) + \exp\left(\frac{-(-x - [z(s) - z(u)])^2 \hat{\tau}}{4(s - u)}\right) \right] dx du \end{aligned} \quad (4.15)$$

Recalling $\omega := -G(V_s)$, this completes the (formal) derivation of the delay differential equation, in view of (4.7), (4.13).

4.2 Numerical algorithm for the delay-differential equation

Let s_0 be an initial time and let $z_0 \in \text{PC}^1((-\infty, s_0])$ be a function specifying a 'history'. We use the notation $z_0 \in \text{PC}^1((-\infty, s_0])$ for z_0 continuous and piecewise C^1 on $(-\infty, s_0]$ (with one-sided derivatives at the breakpoints). Given $a \in \mathbb{R}$, we piecewise linearly extend $z_0(\cdot)$ to a function $z[a](s)$, by setting

$$z[a](s) = z(s_0) + (z'(s_0) + a)(s - s_0) \text{ for } s \geq s_0.$$

Consider the delay functional $W[z]$ given by (4.2) and the error term

$$e(s, a) := \frac{\sqrt{2}}{3} z[a]'(s) - \alpha(\hat{\tau} W[z[a]](s) - q_b^-(z[a](s)); 0) - \gamma,$$

i.e. the extended function $z[a](s)$ satisfies the delay differential equation at time s if and only if $e(s, a) = 0$.

4.2.1 Algorithm 1

Input: An initial time s_0 and a function $z_0 \in \text{PC}^1((-\infty, s_0])$ specifying a 'history', such that $z_0(s)$ satisfies the delay differential equation at $s = s_0$. We do not require that $z_0(s)$ satisfies the delay differential equation at $s < s_0$ (from a practical point of view the algorithm even seems to work if $z_0(s_0)$ does not satisfy the delay differential equation, and quickly converges in forward time s to an actual solution) Let $T > 0$ and consider the interval $[s_0, s_0 + T]$. Let N be an integer such that $h = \frac{T}{N} < h_0$. Denote $s_i := s_0 + ih$, for $i = 0, \dots, N$.

Set $\widehat{z}_0 := z_0(\cdot)$. To construct a numeric solution of the delay differential equation on $[s_0, s_0 + T]$ we proceed along the following step, for $i = 1, \dots, N$

1. Assuming $\widehat{z}_{i-1} \in \text{PC}^1((-\infty, s_{i-1}])$ has been defined on $(-\infty, s_{i-1}]$, consider the extended function $\widehat{z}_{i-1}[a]$. Consider the error term

$$e_i(s, a) := \frac{\sqrt{2}}{3} \widehat{z}_{i-1}[a]'(s) - \alpha(\widehat{\tau}W[\widehat{z}_{i-1}[a]](s_i) - q_b^-(\widehat{z}_{i-1}[a](s_i); 0) - \gamma). \quad (4.17)$$

2. We solve the equation $e_i(s_i, a) = 0$, for a as follows. Existence and uniqueness of the solution $a = a_i^*$ is justified in [39] for $0 < h \ll 1$ (under suitable conditions on the history $\widehat{z}_0(\cdot)$ involving Lipschitz continuity, see [39]).
3. We define $\widehat{z}_i \in \text{PC}^1((-\infty, s_i])$ by

$$\widehat{z}_i := \widehat{z}_{i-1}[a_i^*]|_{(-\infty, s_i]}$$

By construction we have $e_i(s_i, a_i^*) = 0$, which means that $\widehat{z}_i(s)$ satisfies the delay differential equation at $s = s_i$.

Output. Set $\widehat{z} := \widehat{z}_N$. Then (since $e_i(s_i, a_i^*) = 0$ for all i by construction), $\widehat{z}(s)$ solves the delay differential equation at $s = s_i$, for $i = 0, \dots, N$.

In order to implement the algorithm one needs a way to efficiently compute numerically the double integral involved in the delay differential equation. To this end we use the following probabilistic interpretation

$$W[z](s) = \mathbb{E}_{\substack{X \sim \text{Exp}(1) \\ R|X \sim \text{Levy}\left(0, \frac{\hat{\tau}X^2}{2}\right)}} \left[\begin{array}{c} \frac{1}{\hat{\tau}X} z'(s-R)(1 + f_2(z(s-R)))R \\ \exp\left(-\left[\frac{1}{\hat{\tau}} + \frac{\hat{\tau}}{4} \left(\frac{z(s)-z(s-R)}{R}\right)^2\right]R\right) \\ 2 \cosh\left(\frac{1}{2} \hat{\tau} \left(\frac{z(s)-z(s-R)}{R}\right)X\right) \end{array} \right].$$

The probabilistic interpretation can be used to compute the double integral by means of using Monte Carlo integration. The main parameters determining the precision of the algorithm are the number of Monte Carlo samples M per time steps, and the length of each time step h (i.e. the temporal discretization) or equivalently, the temporal resolution $R = \lceil \frac{1}{h} \rceil$, i.e. the number of steps per unit time. Note that the computation time is $\mathcal{O}(MR)$.

4.2.2 Algorithm 2

A slight variation on Algorithm 1, which avoids Monte Carlo integration is based on the implicit form (4.2) of delay-differential equation. The idea is to numerically simulate V_R alongside z_R and involve the estimate of V_R in the evaluation of the error term $e_i(s; a)$ (as in (4.17)).

We start the simulation with an estimate of $V_R(\cdot, s_0)$, which in principle can be obtained from the history $z(s)$, $s \leq s_0$ via (4.14) and (4.15) for $\omega = \mathcal{G}(\partial_s V_R)$. An estimate for $V_R(\cdot, s_0)$ can also be clear from the context (see e.g. example 0 in Section 4.3). In addition to \widehat{z}_0 as described in the initialization step $i = 0$ of Algorithm 1, set $\widehat{V}_{R,0} := V_R(\cdot, s_0)$. As in Algorithm 1, we proceed by iteration for $i = 1, \dots, N$. In the i -th step of the simulation we consider the error

$$e_i(s_i, a) = \frac{\sqrt{2}}{3} (\widehat{z}_{i-1}[a])'(s) - \alpha V(\widehat{z}_{i-1}[a](s_i), s_i; a) - \gamma$$

where $V(\cdot; a)$ is obtained by numerically solving the initial value problem (with $\widehat{V}_{i-1}(\cdot; s_{i-1})$ defined in the previous iteration step $i - 1$)

$$\hat{\tau} \partial_s V = \partial_x^2 V - V + (1 + f_2(x)) \text{sign}(x - \widehat{z}_{i-1}[a](s)), \quad V(\cdot, s_{i-1}; a) = \widehat{V}_{i-1}(\cdot, s_{i-1})$$

for $s \in [s_{i-1}, s_i]$. Solve $e(s_i, a) = 0$ for a , giving $a = a_i^*$ and set

$$\begin{cases} (\widehat{V}_i(\cdot, s), \widehat{z}_i(s)) := (\widehat{V}_{i-1}(\cdot, s), \widehat{z}_{i-1}(s)) & \text{for } s \leq s_{i-1} \\ (\widehat{V}_i(\cdot, s), \widehat{z}_i(s)) := (\widehat{V}(\cdot, s; a_i^*), \widehat{z}_{i-1}[a_i^*](s)) & \text{for } s \in [s_{i-1}, s_i] \end{cases}$$

4.2.3 Algorithm 1 vs Algorithm 2

It is good to keep both Algorithm 1 and Algorithm 2 because they provide two genuinely different numerical routes to the same reduced front-position law, and that difference is useful rather than redundant. Algorithm 1 works directly with the explicit delay functional $W[z]$ and typically evaluates the defining double integral via its probabilistic (Monte–Carlo) interpretation, whereas Algorithm 2 uses the implicit formulation by evolving the auxiliary field V_R through a PDE and coupling it back into the update of the position. Since these approaches have different sources of numerical error—Algorithm 1 is dominated by sampling variance (and time-stepping error), while Algorithm 2 is dominated by deterministic discretization and solver choices—keeping both provides an internal consistency check: when they agree (as in Example 0), this strongly supports both the reduction and the implementation. When they disagree (as in Example 3), the discrepancy is equally informative because it highlights parameter regimes in which one formulation or its discretization is more delicate, thereby aiding diagnosis of instability, stiffness, boundary effects, or insufficient resolution. Finally, the two methods offer complementary practical trade-offs: Algorithm 1 avoids building a full PDE solver and is convenient when one only needs $z(s)$, while Algorithm 2 can be efficient in some regimes, avoids Monte–Carlo sampling entirely, and simultaneously produces $V_R(\cdot, s)$, which is useful for interpreting and validating the front dynamics.

4.3 Numerical exploration of front dynamics

We can now compare the dynamics predicted by the delay equation with direct simulations of the full PDE and explore several qualitatively different regimes. Example 0 considers a front in a heterogeneous medium without

stationary fronts and shows how the heterogeneity modulates the front speed while preserving its direction of motion. Example 1 treats the case $\alpha < 0$ with two stationary fronts and illustrates how travelling fronts connect and interact with these equilibria in agreement with Results 3.9 and 3.10. Example 2 focuses on the homogeneous case $f_2 \equiv 0$ with mixed feedback $\alpha > 0$ and demonstrates direction-reversing fronts that connect different constant-speed travelling waves. Finally, Example 3 introduces a strong localized heterogeneity (outside the rigorous assumptions) that acts as a pair of direction switches and leads to numerically observed periodic front motion, providing an exploratory test of the delay equation beyond the theoretical setting. The corresponding code is available at [40].

Example 0: Travelling front moving with a time-dependent speed $z'(s)$ in the absence of stationary fronts. We consider a compactly supported f_2 . The front enters and passes through the support of f_2 . We set $\alpha = 0.5$, $\gamma = 0.2$, $\hat{\tau} = 1$. We define $f_2(x)$ as a piecewise polynomial defined on $[-3, 15]$. To this end, we sample the function

$$(y - 3) \sin(1 + 14(y - 3)^3) \exp(-1.2|y - 3|)$$

for the y -values $y = 3, 4, 5, 6, 7, 8, 9$ and then use MATLAB's `makima` interpolation to construct a piecewise polynomial defined on $[3, 10]$ satisfying $f_2(3) = f_2(10) = 0$. The sampled values $y = 4, 5, 6, 7, 8, 9$ (approximately) specify the local minima and maxima of the resulting f_2 . For $x \leq 3$ and $x \geq 10$ we set $f_2(x) = 0$.

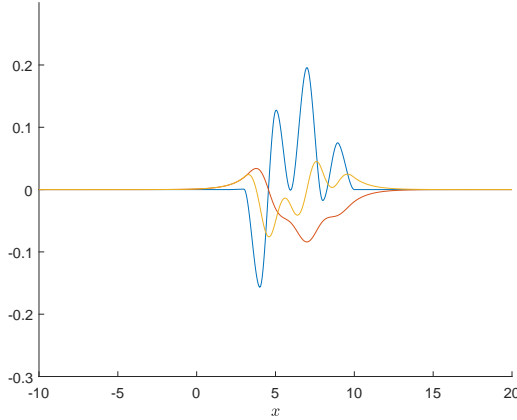


Figure 5: $f_2(x)$ (in black), $v_b^-(x; 0) + 1$ (orange) and $q_b^-(x; 0)$ (yellow). The shape of f_2 is chosen such that it involves multiple local minima and maxima. The corresponding $q_b^-(x; 0)$ also fluctuates and we expect the front velocity to change over time as well, in an interesting way. The parameter γ is chosen to avoid the presence of stationary fronts, i.e. intersections of the graph of $q_b^-(\cdot; 0)$ with the horizontal line at height $\frac{\gamma}{\alpha} = 0.4$.

When $f_2 = 0$, there exists a unique constant-speed travelling front. In the singular limit, the speed is given by $c \approx 0.83$. Introducing f_2 , we expect that outside the support of f_2 the dynamics are close to the dynamics of the constant-coefficient model; in particular, the singular limit of the front velocity will be close to 0.83. We simulate the PDE for various values of $0 < \varepsilon \ll 1$ (using MATLAB's `pdepe`), with an initial condition (U_0, V_0) starting at position $z_0 = -2.5$ (outside the support of f_2). That is, $z_0 = -2.5$ is the starting position, in the sense that $U_0(z_0) = 0$. The initial condition is constructed by first simulating the constant-coefficient PDE. The fronts travel to the right with positive speed, and pass through the support of f_2 . The front speed remains positive, but

is not constant and fluctuates when the front is in the vicinity of the support of f_2 .

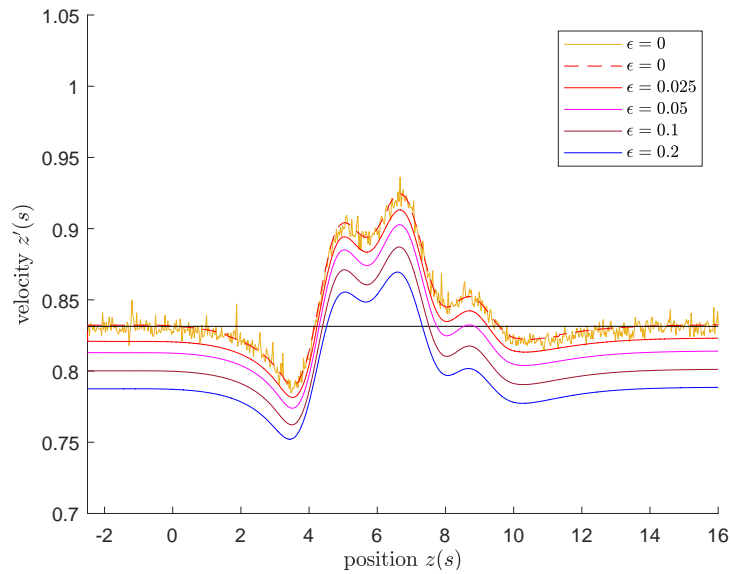


Figure 6: Simulated position against velocity for the singular limit $\varepsilon = 0$ (delay equation) and for various $\varepsilon > 0$. For $\varepsilon = 0$ the figure shows both the Monte Carlo approach (Section 4.2.1) to simulating the delay-differential equation, as well as the approach in Section 4.2.2 based on the delay-differential equation in implicit form. The two approaches closely agree in the present example. For simulations of the delay-differential equation using the Monte Carlo approach we use $M = 10^5$ Monte Carlo samples, and a time discretization of 30 steps per time unit $s = 1$.

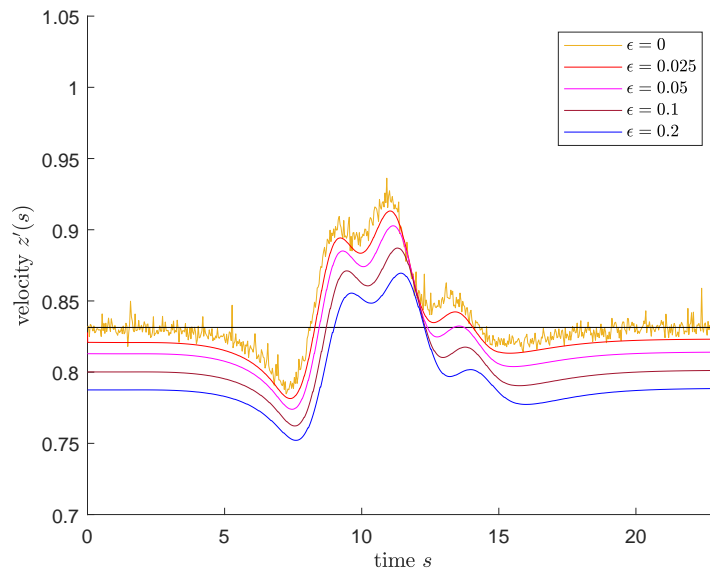


Figure 7: Time against simulated velocity for the singular limit $\varepsilon = 0$ (delay equation) and for various $\varepsilon > 0$.

Example 1: Travelling front for $\alpha < 0$ in the presence of stationary fronts. The aim of the present example is to illustrate Result 3.10, describing the interaction of travelling fronts and stationary fronts for

positive feedback $\alpha < 0$. To this end we consider the parameter values $\alpha = -2$, $\gamma = -0.2$, $\hat{\tau} = 1$, and

$$f_2(x) = 0.3 \exp(-0.5(x + 0.1)^2) + 0.33 \exp(-2(x + 1.5)^2) - 0.53 \exp(-2(x + 0.75)^2) \\ + 0.25 \exp(-4(x - 0.1)^2) - 0.4 \exp(-3(x - 1)^2).$$

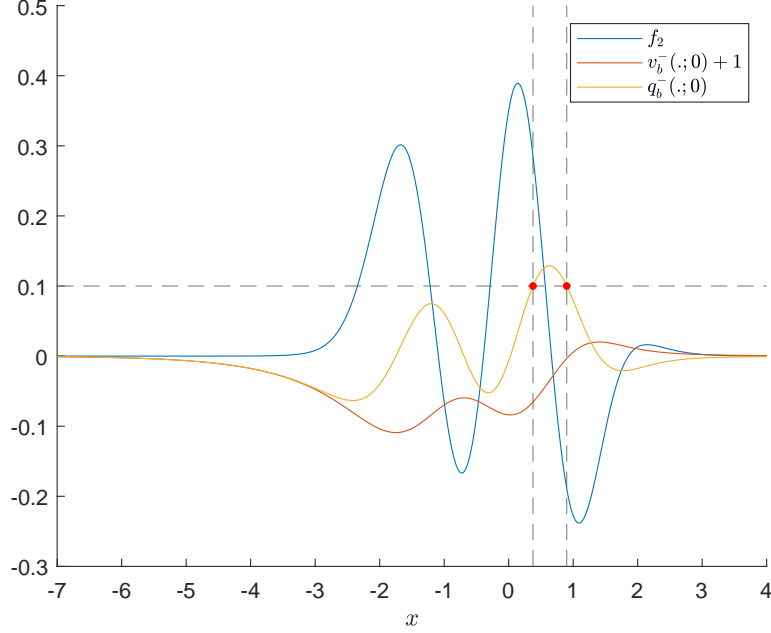


Figure 8: $f_2(x)$, $v_b^-(x; 0) + 1$ and $q_b^-(x; 0)$. The figure also indicates the singular limit positions of the stationary fronts given by the intersection points of $q_b^-(\cdot; 0)$ with the horizontal line $\frac{\gamma}{\alpha} = 0.1$.

For $0 < \varepsilon \ll 1$, there exist two stationary fronts $\text{SF}_i(\varepsilon)$ with positions $z_{0,i}(\varepsilon)$, $i = 1, 2$, where by Result 3.3 the singular limit positions $z_{0,i}(0)$ are given by the solutions z_0 of the equation $q_b^-(z_0; 0) = \frac{\gamma}{\alpha} = 0.1$. Approximately, we have $z_{0,1}(0) \approx 0.38$ and $z_{0,2}(0) \approx 0.90$. The stationary front at position $z_{0,1}(\varepsilon)$ is unstable (since $(q_b^-)'(z_{0,1}(0); \delta_0, 0) > 0$) and the stationary front at position $z_{0,2}(\varepsilon)$ is stable (see Result 3.10).

To generate an initial condition at a given target position $z_0 \in \mathbb{R}$ (in particular in the vicinity of the unstable stationary front for $\varepsilon > 0$), we use the following algorithm. Let $z_0 \in \mathbb{R}$ be the target position where we want to construct an initial condition (U_0, V_0) . Start with an initial condition $(U_{0,0}, V_{0,0})$ which has a front-like shape (i.e. connecting the background states and having a single interface). Taking a sequence $(T_i)_i$, $T_i > 0$, we iteratively construct initial conditions $(U_{0,i}, V_{0,i})$ by solving the PDE (1.4) with initial condition $(U_{0,i-1}, V_{0,i-1})$ up to time T_i , and then shifting the resulting solution $(U, V)_{i-1}(x, T_i)$ in space to the position z_0 , i.e. $(U_{0,i}, V_{0,i})(x) := (U, V)_{i-1}(x - z_0 + z_{i-1}(T_i), T_i)$. The main idea is to let $T_i \rightarrow 0$ while also ensuring that $\sum_i T_i$ is not too small in order to filter out transient dynamics.

We choose to work with the following sequence of times $T_1 = 1$, $T_2 = 1$, $T_3 = 1$, $T_4 = 0.5$, $T_5 = 0.5$, $T_6 = 0.3$, $T_7 = 0.2$.

For $\varepsilon = 0.05$ we estimate that the position $z_{0,1}(0.05)$ of the stationary front is contained in the interval $[0.37577, 0.37609]$. The estimate arises from the fact that we constructed an initial condition $(U_{0,a}, V_{0,a})$ at

position 0.37577 which ends up generating a front travelling to the left, and an initial condition $(U_{0,b}, V_{0,b})$ at position 0.37609 which generates a front travelling to the right. Likewise, for $\varepsilon = 0.1$ we estimate that $z_{0,1}(0.1)$ is contained in the interval $[0.37714, 0.38452]$.

The position of the stable stationary front is (surprisingly) a bit harder to estimate. On the one hand, stability implies that approaching fronts from the right and left are attracted, and consequently it appears that the position can be estimated in this way by tracking approaching fronts numerically for long enough. However, the numerics involve a discretization of space, and the position of the numerical front is confined to this grid. Hence, to estimate the position of the stationary front more precisely, one needs to increase the resolution of the grid, which quickly increases computation time.

Figure 9 and Figure 10 illustrate a travelling front connecting stationary fronts SF_1 in backward time and SF_2 in forward time. Both the position $z(s)$ and the front velocity $z'(s)$ closely agree with the associated singular position and velocity given by simulating the delay-differential equation. In particular, when looking only at the front position $z(s)$ (Figure 10), the comparison between $\varepsilon = 0.1$ and $\varepsilon = 0$ is already remarkably precise, which is why $\varepsilon = 0.05$ is not included in this figure. On the other hand, the comparison for the front velocity $z'(s)$ with the delay-differential equation (Figure 9) noticeably improves for $\varepsilon = 0.05$ compared to $\varepsilon = 0.1$. Figures 11 and Figure 12 extend the simulation by including other travelling fronts besides the travelling front connecting the stationary fronts. Specifically, a travelling front is included which travels away from the unstable stationary front SF_1 to the left, and a travelling front which approaches the stable stationary front SF_2 from the right.

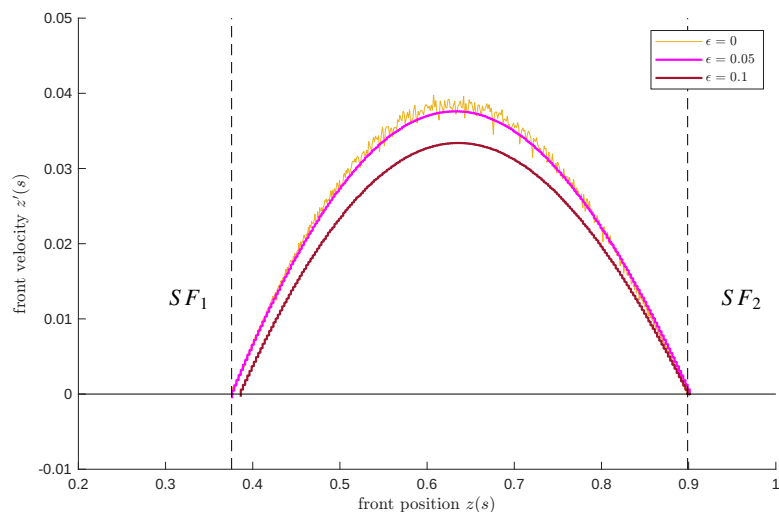


Figure 9: Simulated position against velocity, delay-differential equation, $\varepsilon = 0.05$ and $\varepsilon = 0.1$. The dashed vertical lines indicate the singular limit positions of the stationary fronts. For simulation of the delay-differential equation we use Algorithm 1 in Section 4.2.1 with $M = 10^5$ Monte Carlo samples, and a time discretization of 30 steps per time unit $s = 1$.

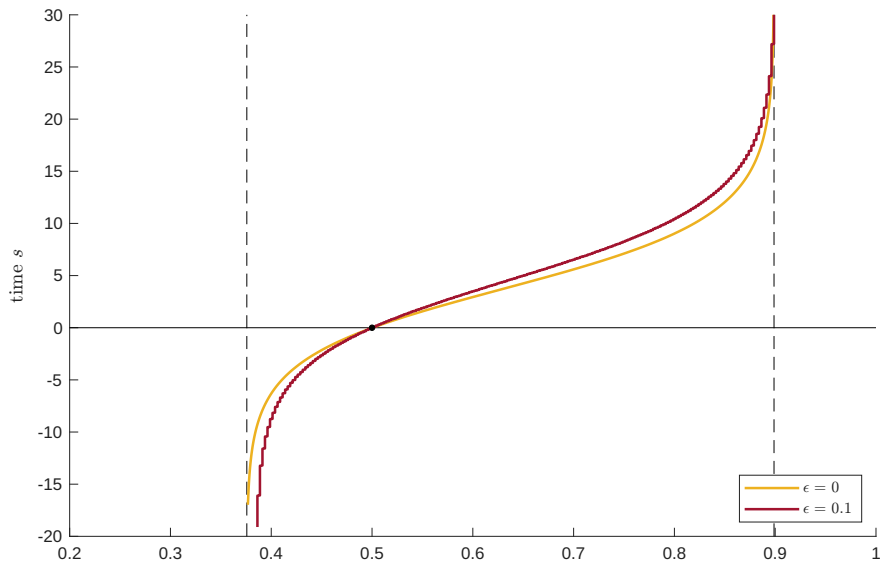


Figure 10: Simulated position against time, delay-differential equation and $\varepsilon = 0.1$. The dashed lines indicate the singular limit positions of the stationary fronts. To compare the delay-differential equation to the PDE (1.4) for $\varepsilon = 0.1$, we arrange (using translational symmetry in time) that the (time/position) trajectories pass through the common point $(z, s) = (0.5, 0)$.

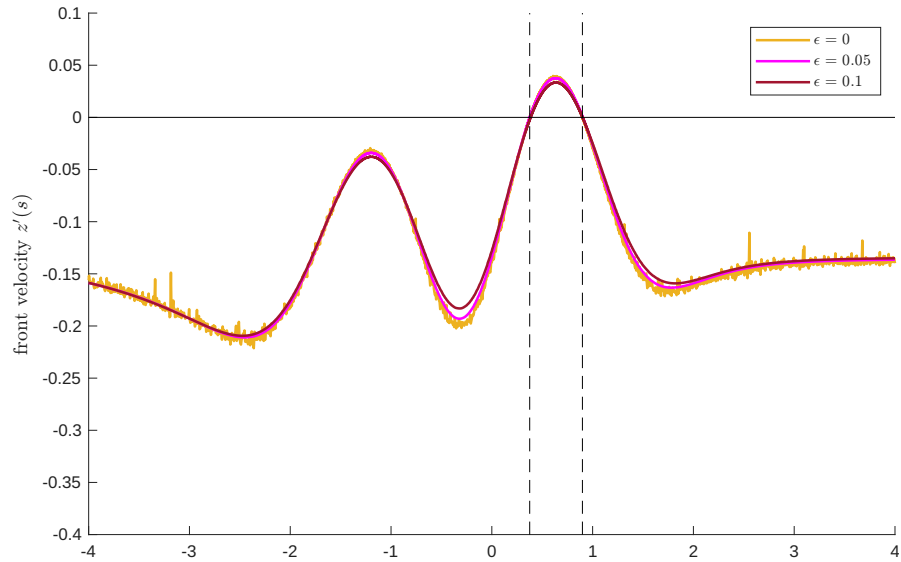


Figure 11: Simulated position against velocity, delay-differential equation, $\varepsilon = 0.05$ and $\varepsilon = 0.1$. In addition to the travelling fronts connecting the unstable and stable stationary fronts shown in Figure 9, the present figure shows additional travelling fronts. Specifically, a travelling front which travels away from the unstable stationary front SF_1 to the left, and a travelling front which approaches the stable stationary front SF_2 from the right.

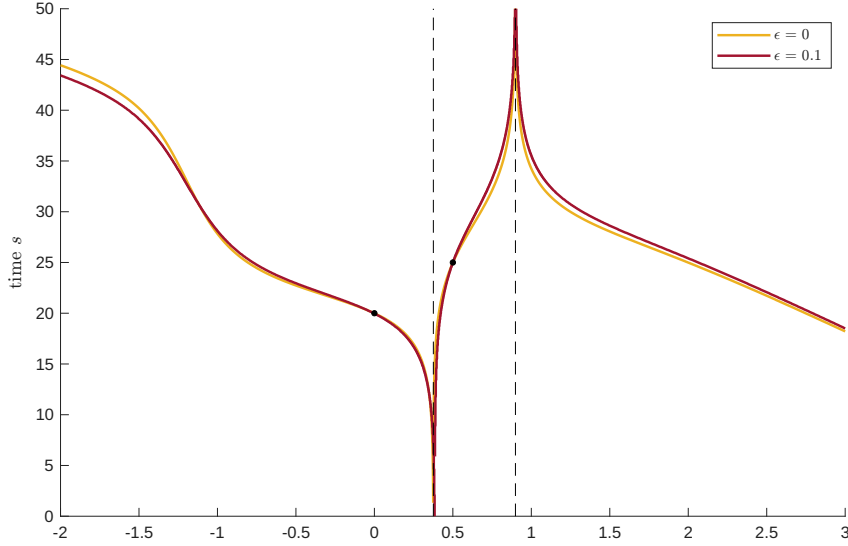


Figure 12: Simulated position against time, delay-differential equation, $\varepsilon = 0.05$ and $\varepsilon = 0.1$. To compare the delay-differential equation to the PDE (1.4) for $\varepsilon = 0.1$, we arrange (using translational symmetry in time) that the (time/position) trajectories pass through the common point $(z, s) = (0.5, 25)$.

Example 2: Direction-reversing front for $\alpha > 0$ and $f_2 = 0$. We set $\hat{\tau} = 1$, $\gamma = 0.2$. Let α_{bp} be given by

$$\alpha_{bp} = \left(\frac{\sqrt{2}}{3} c_{bp} - \gamma \right) \frac{\sqrt{4 + c_{bp}^2 \hat{\tau}^2}}{c_{bp} \hat{\tau}} \approx 1.489, \quad c_{bp} = - \left(\frac{12\gamma}{\sqrt{2}\hat{\tau}^2} \right)^{\frac{1}{3}}.$$

For $\alpha < \alpha_{bp}$, the algebraic equation (4.6) has a unique solution c which corresponds to (up to translation in space) a unique constant-speed travelling front for the PDE (1.4) for $0 < \varepsilon \ll 1$. For $\alpha > \alpha_{bp}$, (4.6) has three solutions $c_m < c_0 < c_p$, which for $0 < \varepsilon \ll 1$ correspond to travelling fronts with speeds $c_m(\varepsilon) < c_0(\varepsilon) < 0 < c_p(\varepsilon)$.

For the present example, we take $\alpha = 2.5 > \alpha_{bp}$. We also fix $\varepsilon = 0.1$ and compare it with the singular limit $\varepsilon = 0$.

One can show that the delay-differential equation [39, Chapter 5] has an entire solution $z(s)$, which satisfies $z'(s) \rightarrow c_0 < 0$ as $s \rightarrow -\infty$, $z'(s) \rightarrow c_p > 0$ as $s \rightarrow \infty$, and $z'(s)$ is increasing in s . That is, in the singular limit $\varepsilon = 0$ there exists a travelling front which changes direction, i.e. it initially travels to the left with negative speed (asymptotic to c_0 in backward time) and eventually approaches the positive speed $c_p > 0$. In this example we explore numerically whether the PDE (1.4) has a similar direction-reversing travelling front solution for $0 < \varepsilon \ll 1$ (approaching $c_0(\varepsilon)$ and $c_p(\varepsilon)$ in backward, respectively forward time).

For setting up the simulation, the main challenge is to construct the initial condition (U_0, V_0) , which should be close to the front profile of the unstable constant-speed travelling front with speed $c_0(\varepsilon)$. To this end we consider the singularly perturbed system of ODEs for (u, p, v, q) corresponding (in the fast scaling ξ) to

the co-moving frame $\xi = \frac{x-cs}{\varepsilon}$. For a given value of c , there exists a unique orbit (standardized such that $u(0) = 0$), which is forward asymptotic to the (independent of x , since in the present example $f_2 = 0$) background state $(u_b^+(\varepsilon), 0, u_b^+(\varepsilon), 0)$ and a unique orbit which is backward asymptotic to $(u_b^-(\varepsilon), 0, u_b^-(\varepsilon), 0)$. For $c = c_m(\varepsilon), c_0(\varepsilon), c_p(\varepsilon)$, these forward and backward orbits match at $z_0 = 0$, and form a heteroclinic. We numerically determine the value $c_0(\varepsilon)$ which gives rise to a heteroclinic orbit. To this end we identify locally invariant manifolds $\mathcal{M}_\varepsilon^\pm$ and restrict first to the one-parameter family of orbits which lie in the intersection of $W^u(\mathcal{M}_\varepsilon^-)$ and $W^s(\mathcal{M}_\varepsilon^+)$. To find this family of orbits we use an approximation of $\mathcal{M}_\varepsilon^\pm$ (the first order approximation in ε already works well), and a ‘shooting’ approach (tracking multiple orbits and investigating how closely they approach $\mathcal{M}_\varepsilon^\pm$). The resulting family is described by $u_0 = 0$ and (p_0, v_0) being a function of q . We then use a second layer of ‘shooting’ to investigate, for fixed c , which forward orbit in (the one-parameter family) $W^s(\mathcal{M}_\varepsilon^-) \cap W^u(\mathcal{M}_\varepsilon^+)$ converges to the positive background state, and which backward orbit converges to the negative background state. Lastly, using a bisection approach we can compute the value of c where the forward and backward orbits match. According to the numerical results, $c_0(\varepsilon)$ (for $\varepsilon = 0.1$) is contained in the interval $(-0.309375, -0.30875)$ (for comparison the singular limit velocity is given by $c_0(0) = -0.261792$). We now consider the following cases.

To construct an initial condition (U_0, V_0) such that the solution of the PDE (1.4) will reverse the direction of travelling, we take c slightly larger than $c_0(\varepsilon)$ and define (U_0, V_0) by means of concatenating the forward orbit converging to the positive background state with the backward orbit converging to the negative background state. How long the velocity $z'(s)$ stays close to $c_0(\varepsilon)$ before moving away from it depends on how close c is to $c_0(\varepsilon)$, as well as on other numerical factors (i.e. in the shooting algorithm described above).

To construct an initial condition (U_0, V_0) for which the solution of the PDE will not reverse direction but instead converge to the stable travelling front with speed $c_m(\varepsilon)$, we take c slightly smaller than $c_0(\varepsilon)$ and again concatenate forward and backward orbits.

For $\varepsilon = 0$, we simulate the delay-differential equation, specifying the history to be $z_0 = 0$ and $z'(s) = c_0(0)$ for $s \leq 0$. Using the Monte Carlo approach for evaluating the delay functional, it depends on the specific sample realizations (i.e. seed for the pseudo random number generator) whether the velocity $z'(s)$ ends up converging to $c_p(0)$ or $c_m(0)$. How long the solution of the delay-differential equation stays close to $c_m(0)$ before splitting up depends (in particular) on the number of Monte Carlo samples, and the time discretization.

In summary, we obtain two numerical PDE solutions for $\varepsilon = 0.1$, one which connects the velocities $c_0(\varepsilon) < 0$ and $c_p(\varepsilon) > 0$ (and in particular reverses its direction of travelling) and a second solution which connects the velocities $c_0(\varepsilon) < 0$ and $c_m(\varepsilon) < 0$. For $\varepsilon = 0$ we obtain similar solutions of the delay-differential equation. Figures 13, 14, 15 depict the position and velocity compared for $\varepsilon = 0$ and $\varepsilon = 0.1$.

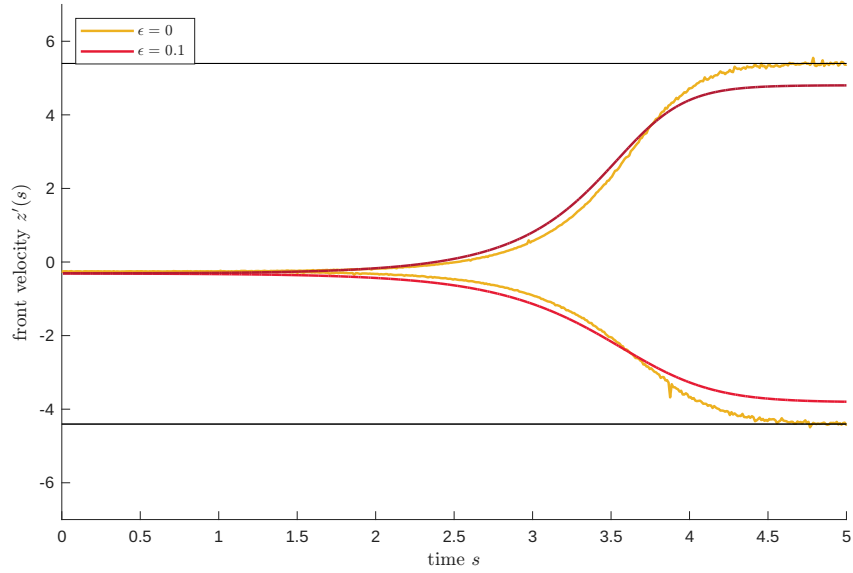


Figure 13: Simulated velocity against time, delay-differential equation and $\varepsilon = 0.1$. For simulation of the delay-differential equation we use Algorithm 1 in Section 4.2.1 with $M = 1.5 \times 10^5$ Monte Carlo samples, and a time discretization of 100 steps per time unit $s = 1$. The horizontal lines indicate the singular limit of the stable speeds $c_m(0) < 0$ and $c_p(0) > 0$.

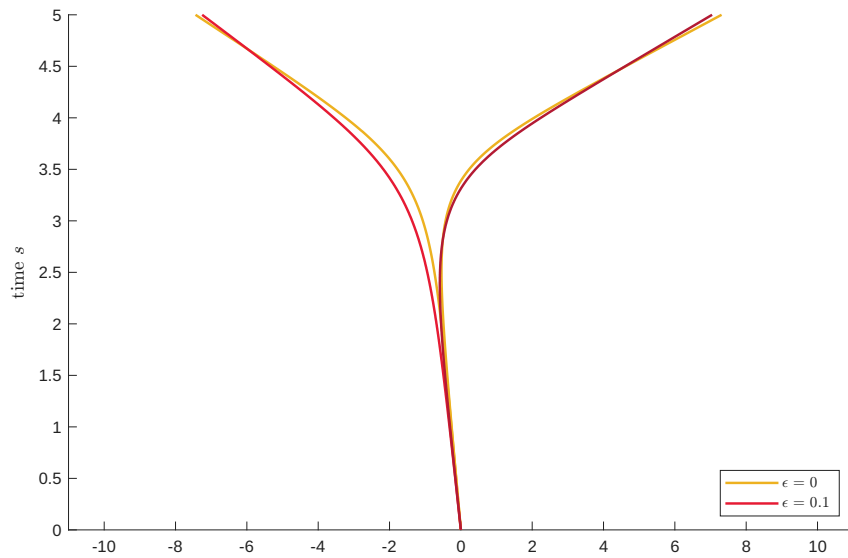


Figure 14: Simulated position against time, delay-differential equation and $\varepsilon = 0.1$.

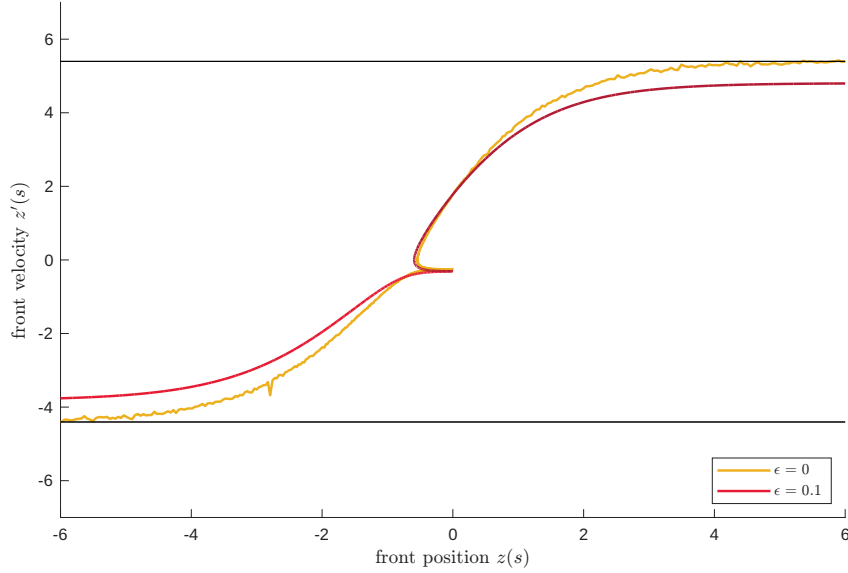


Figure 15: Simulated position against velocity, delay-differential equation and $\varepsilon = 0.1$. The horizontal lines indicate the singular limit of the stable speeds $c_m(0) < 0$ and $c_p(0) > 0$.

Example 3: Direction switches and periodic front. A periodic front for the parameter values $(\alpha, \gamma, \hat{\tau})$ of Example 2 when the inhomogeneity f_2 is introduced.

Unlike Examples 0 and 1, which illustrate theoretical results (i.e. Result 4.1 and Result 3.10, respectively), and Example 2 which illustrates partial results (i.e. the existence of direction-reversing entire solutions for the delay-differential equation ($\varepsilon = 0$), but not for the PDE (1.4) for $\varepsilon > 0$), the present example is purely exploratory (in the sense that it is not backed up by theoretical results). In fact the f_2 which we will work with does not satisfy Assumptions 1.1.

The delay-differential equation is of the form

$$\gamma + \alpha(\hat{\tau}W[z](s) - q_b^-(z(s); 0)) = \frac{\sqrt{2}}{3}z'(s).$$

In particular, it appears that sudden large changes in q_b^- might have a similar impact on the velocity $z'(s)$. This raises the question whether a localised inhomogeneity f_2 might act as a ‘direction switch’, i.e. cause approaching fronts to reverse their direction.

We explore this question in the context of the parameters in Example 2, where we discussed that in the absence of f_2 there exist stable speeds $c_m(\varepsilon) < 0$ and $c_p(\varepsilon) > 0$. We introduce the following f_2 given by two localized pulses at positions $z = \pm 11$

$$f_2(x) = -\rho \exp(-40(x + 11)^2) - \rho \exp(-40(x - 11)^2).$$

We set $\rho = 12$. The graph of the corresponding $q_b^-(\cdot; 0)$ has large changes in the vicinity of positions $z = \pm 11$ of the pulses and is close to 0 everywhere else.

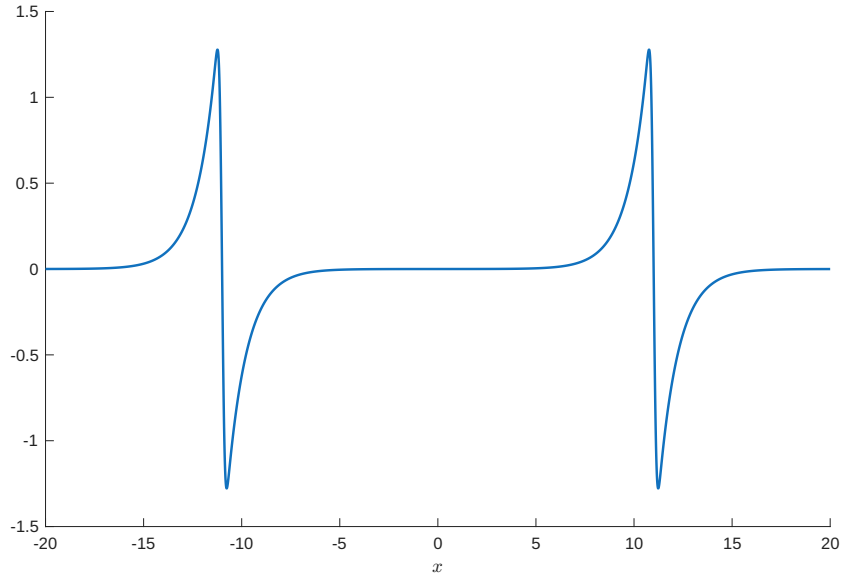


Figure 16: Graph of $q_b^-(x; 0)$. The graph exhibits two localized regions where it changes in a rapid way. The intention of the design is to construct direction switches which reverse the direction of approaching fronts, and trap them in a compact space given by the space between the two switches. The choice for the scaling $\rho = 12$ in the definition of f_2 comes from the fact that it makes the switches strong enough for this purpose. For example, reversing a front approaching the Gaussian pulse at $z = -11$ from the left seems to require taking ρ around 4.

Near $z_0 = 0$ (far away from ± 11) we expect the front dynamics to be close to the constant-coefficient model where $f_2 = 0$. Consider a front travelling to the left away from $z_0 = 0$ with speed close to $c_m(\varepsilon) < 0$. This front approaches $z = -11$ from the right and will encounter the large negative local minimum of q_b^- . Given the sudden decrease of q_b^- , $z'(s)$ might quickly increase as a response, and if the drop in q_b^- is large enough, $z'(s)$ might become positive, i.e. the front reverses direction.

Likewise, consider a front travelling to the right away from $z_0 = 0$ and towards $z = 11$ with speed close to $c_p(\varepsilon)$. This front will encounter the large local maximum of q_b^- . Consequently, the front speed $z'(s)$ might decrease, and could become negative.

The numerical results confirm expectations. Figure 18 shows the simulated front position $z(s)$ against time and suggests that the pulses placed at positions $z = \pm 11$ act as direction switches as intended. The change of direction occurs around $z = \pm 10$. In particular, the front position is trapped in the compact interval $[-11, 11]$. A periodic front seems to emerge as a consequence of the two direction switches.

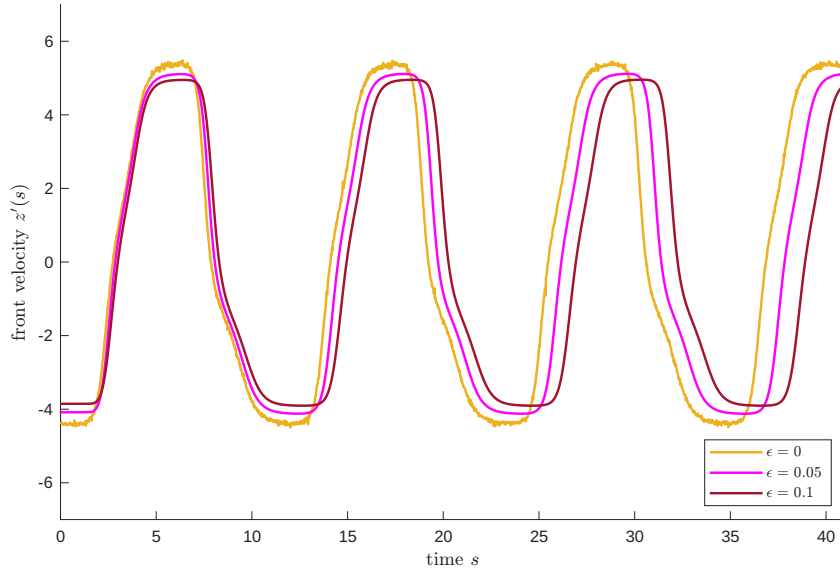


Figure 17: Simulated velocity against time, delay-differential equation, $\epsilon = 0.05$ and $\epsilon = 0.1$. For the delay-differential equation we use Algorithm 1 in Section 4.2.1 with $M = 1.5 \times 10^5$ Monte Carlo samples and a time discretization of 40 steps per time unit $s = 1$. In addition we also explored Algorithm 2 in Section 4.2.2 (not shown) based on the implicit form of the delay-differential equation, but unlike in Example 0, Algorithm 2 does not match the results of Algorithm 1 and in fact does not produce an orbit which appears periodic. The underlying theoretical and/or numerical reasons why Algorithm 2 exhibits behaviour that appears ‘irregular’ are currently unknown.

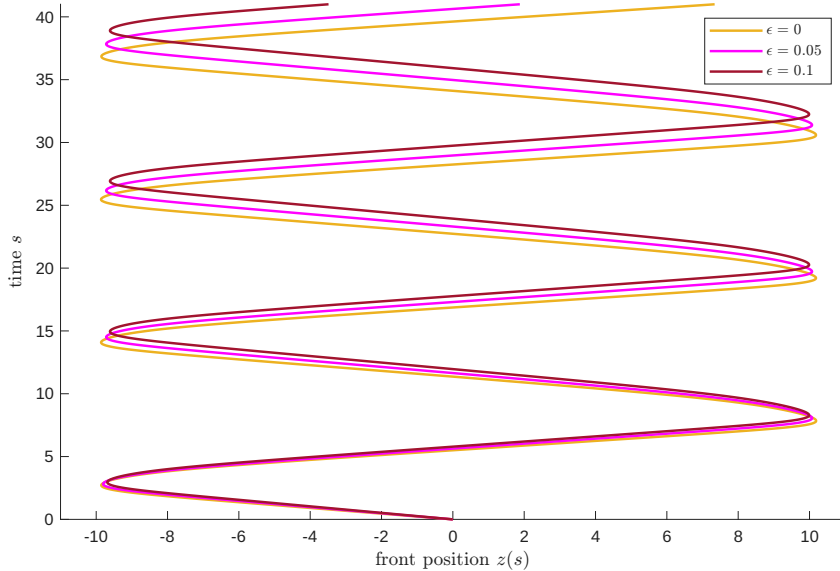


Figure 18: Simulated position against time, delay-differential equation, $\epsilon = 0.05$ and $\epsilon = 0.1$.

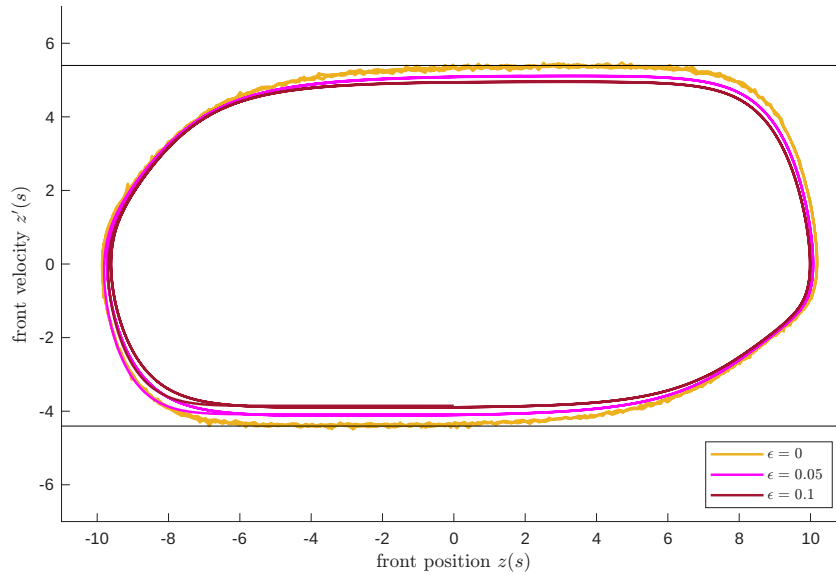


Figure 19: Simulated position against velocity, delay-differential equation, $\epsilon = 0.05$ and $\epsilon = 0.1$.

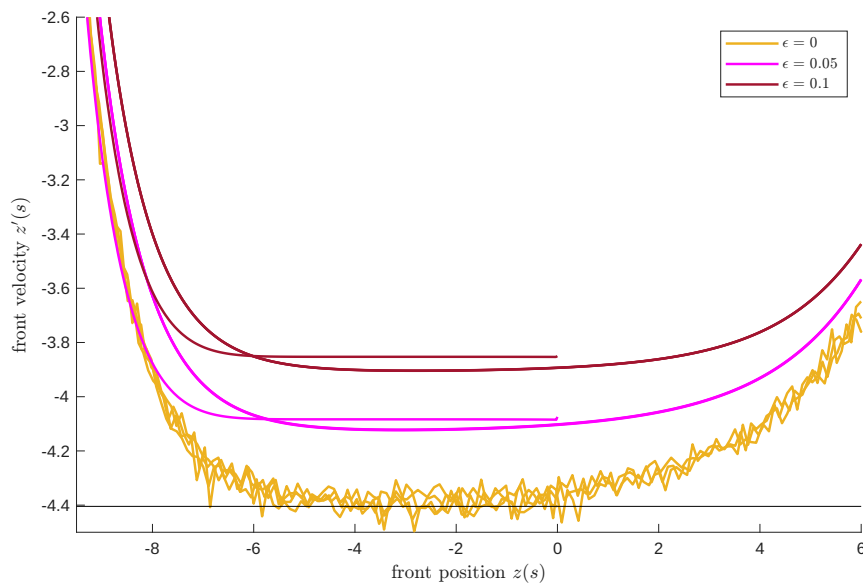


Figure 20: Simulated position against velocity, delay-differential equation, $\epsilon = 0.05$ and $\epsilon = 0.1$. The figure shows a zoomed-in version of Figure 19. The figure shows that (due to transient dynamics) the initial part of the front position/velocity trajectory for $\epsilon = 0$ and $\epsilon = 0.1$ deviates from the periodic orbit which seems to be approached eventually. More specifically, the deviation is particularly noticeable when the position/velocity trajectory approaches the southwest region of the domain for the first time. Interestingly, the simulated path for the delay-differential equation ($\epsilon = 0$) does not appear to have a noticeable initial transient phase.

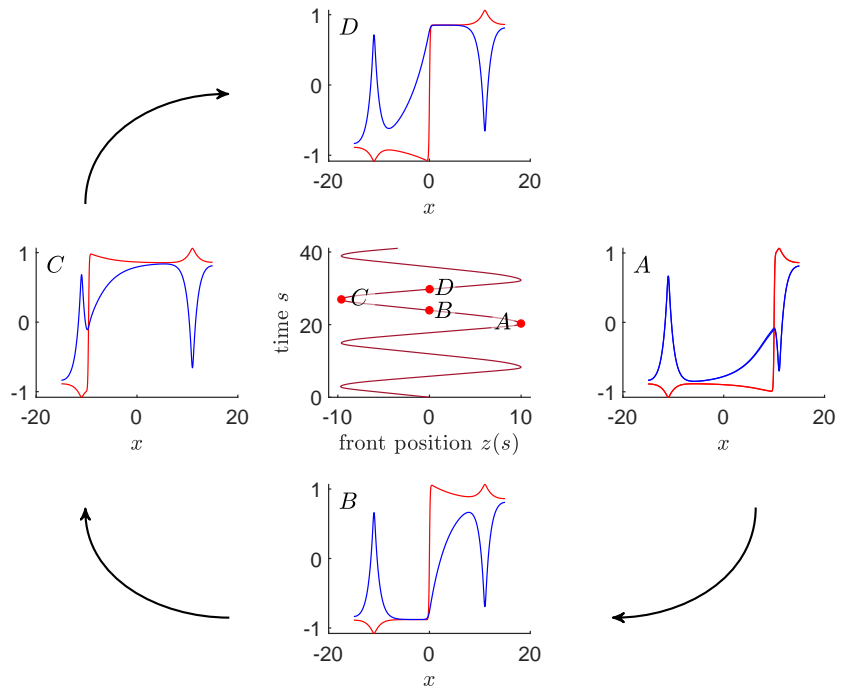


Figure 21: Front profile of solution (U, V) at various points A, B, C, D of the simulated periodic orbit for $\varepsilon = 0.1$. The U -component is shown in red and the V -component is shown in black.

5 Summary and outlook

We have demonstrated that (1.1) exhibits bi-stability, characterized by two stable stationary background states that vary in space due to the presence of f_1, f_2 and further give rise to stationary and travelling front solutions that connect them.

The construction of stationary background states in the stationary wave ODE (2.3) needed an extension of Fenichel theory to the general non-autonomous case (that is, going beyond [12] to include also unstable directions) combined with the theory of exponential dichotomies. Using a Melnikov-type argument for (2.3) gave also a leading order existence condition for stationary front solutions (3.1) that resembles the one for the constant-coefficient case (1.3), the difference being that, for fixed parameter settings, the possible front positions x_0 are fixed (contrasting with the translation-invariant case of constant-coefficient equations). Travelling front solutions have a richer structure than their counterparts in the constant-coefficient case: their interfaces move non-uniformly through the motionless heterogeneous background states, which makes the usual travelling wave ansatz hopeless. Upon carefully defining them along their stationary version and numerical observations (see Definition 3.1), it turns out that one can prove (i) their existence from a specific set-up of the corresponding initial value problem (leading to initialised fronts as in Definition 3.5) and (ii) their existence for all $t \in \mathbb{R}$ (leading to entire front solutions as in Definition 3.2). The main novelty of the proof for the IVP lies in tracking the time evolution of the time-derivatives $(\partial_t U, \partial_t V)$ which are bi-asymptotic to zero as $x \rightarrow \pm\infty$ for each fixed t (since the background states are motionless even for travelling front solutions). The proof of the existence of entire solutions is built on the result for the IVP and uses the construction of a localised co-moving frame and the Arzela-Ascoli theorem. The exposition closes with a short formal derivation of a delay-differential equation (4.1) that describes the temporal evolution of the front position (in the sense of Definition 3.8). We briefly sketch a numerical algorithm to solve it and give various examples, both for cases where its validity can be proven rigorously and cases where its validity is expected but not proven. All proofs can be found in [39] and will also be subject of follow-up articles for which the present article serves as overview.

Future research will further generalize the obtained results to other settings with particular interest in treating also nonlinear slow equations, that is, the $+U$ in the V -equation in (1.1) replaced by $F(U, V)$. Furthermore, a careful study of the dynamics exhibited by the delay-differential equation (4.1) will be of interest, but is expected to be challenging due to the difficult type of delay differential equation. Another immediate question is its relation with the traditional approach of deriving reduced ODEs for the dynamic position using a rigorous center manifold reduction (CMR)(for a "collective coordinates type" approach). This is especially interesting since the derivation of (4.1) made no smallness assumption on z , which one does when constructing travelling fronts as bifurcating from stationary ones. Note that, the conventional CMR approach for (1.1) would need control over the spectrum of the operator obtained from linearisation around stationary fronts. This is, in general, difficult unless one enforces smallness assumptions for f_1, f_2 or assumes them to be periodic or spatially localised (as done in [3] for the stability of pulses). The derivation of the delay-differential equation completely circumvents this difficulty.

Further capitalising on the derivation of the delay-differential equation that avoids intricate spectral problems, a promising direction is to use this approach for interacting multi-front and pulse solutions under the influence of spatial heterogeneity. Going beyond the 1-D case, a promising direction is the study of 2-D front solutions and more complicated 2-D patterns such as the tracking of spiral wave tips in reaction-diffusion systems (as given, e.g. in [1, 2, 33, 41]) with applications, e.g. in the modelling of cardiac dynamics where heterogeneities are believed to play a major role.

References

- [1] Barkley, D. Euclidean symmetry and the dynamics of rotating spiral waves. Physical Review Letters **72**(1):164–167 (1994). doi:10.1103/PhysRevLett.72.164
- [2] Barkley, D. and Kevrekidis, I.G. A dynamical systems approach to spiral wave dynamics. Chaos: An Interdisciplinary Journal of Nonlinear Science **4**(3):453–460 (1994). doi:10.1063/1.166023
- [3] Bastiaansen, R., Chirilus-Bruckner, M. and Doelman, A. Pulse solutions for an extended Klausmeier model with spatially varying coefficients. SIAM Journal on Applied Dynamical Systems **19**(1) (2020). doi:10.1137/19M1255665. URL <https://doi.org/10.1137/19M1255665>
- [4] Bastiaansen, R. and Doelman, A. The dynamics of disappearing pulses in a singularly perturbed reaction-diffusion system with parameters that vary in time and space. Physica D: Nonlinear Phenomena **388**:45–72 (2019). doi:10.1016/j.physd.2018.09.003
- [5] Bastiaansen, R., Doelman, A. and Kaper, T. Multi-front dynamics in spatially inhomogeneous Allen-Cahn equations (2025). doi:10.48550/arXiv.2501.16195. arXiv:2501.16195, URL <https://doi.org/10.48550/arXiv.2501.16195>
- [6] Chirilus-Bruckner, M. Front propagation in a spatially heterogeneous reaction-diffusion system (2026). doi:10.5281/zenodo.18769174. URL <https://doi.org/10.5281/zenodo.18769174>
- [7] Chirilus-Bruckner, M., Doelman, A., van Heijster, P. and Rademacher, J.D. Butterfly catastrophe for fronts in a threecomponent reactiondiffusion system. Journal of Nonlinear Science **25**(1):87–129 (2015). doi:10.1007/s00332-014-9202-2
- [8] Chirilus-Bruckner, M., van Heijster, P., Ikeda, H. and Rademacher, J.D. Unfolding symmetric Bogdanov-Takens bifurcations for front dynamics in a reactiondiffusion system. Journal of Nonlinear Science **29**(6):2911–2953 (2019). doi:10.1007/s00332-018-9479-8
- [9] Chirilus-Bruckner, M., van Heijster, P. and Rademacher, J. Chaotic motion and singularity structures of front solutions in multi-component FitzHugh-Nagumo-type systems (2024). doi:10.48550/arXiv.2406.04458. arXiv:2406.04458, URL <https://doi.org/10.48550/arXiv.2406.04458>
- [10] Coppel, W. Dichotomies in Stability Theory, vol. 629 of Lecture Notes in Mathematics. Springer, Berlin, Heidelberg (1978). ISBN 978-3-540-35976-0. doi:10.1007/BFb0067780. URL <https://doi.org/10.1007/BFb0067780>
- [11] Doelman, A., van Heijster, P. and Kaper, T.J. Pulse dynamics in a three-component system: Existence analysis. Journal of Dynamics and Differential Equations **21**(1):73–115 (2009). doi:10.1007/s10884-008-9125-2
- [12] Eldering, J. Persistence of noncompact normally hyperbolic invariant manifolds in bounded geometry. Comptes Rendus Mathématique **350**(11–12) (2012). doi:10.1016/j.crma.2012.06.009. URL <http://dx.doi.org/10.1016/j.crma.2012.06.009>
- [13] Fenichel, N. Asymptotic stability with rate conditions. Indiana University Mathematics Journal **23**(12) (1974). doi:10.1512/iumj.1974.23.23090. URL <http://www.jstor.org/stable/24890716>

- [14] Fenichel, N. Asymptotic stability with rate conditions ii. Indiana University Mathematics Journal **26**(1) (1977). doi:10.1512/iumj.1977.26.26006. URL <http://www.jstor.org/stable/24891324>
- [15] Fenichel, N. Geometric singular perturbation theory for ordinary differential equations. Journal of Differential Equations **31**(1) (1979). doi:10.1016/0022-0396(79)90152-9. URL [https://doi.org/10.1016/0022-0396\(79\)90152-9](https://doi.org/10.1016/0022-0396(79)90152-9)
- [16] Fenichel, N. Hyperbolicity and exponential dichotomy for dynamical systems. In C. Jones, U. Kirchgraber and H. Walther (eds.), Dynamics Reported. New Series, vol. 5. Springer, Berlin, Heidelberg (1996). doi:10.1007/978-3-642-79931-0_1. URL https://doi.org/10.1007/978-3-642-79931-0_1
- [17] van Heijster, P., Doelman, A. and Kaper, T.J. Pulse dynamics in a three-component system: Stability and bifurcation analysis. Physica D **237**(16):3335–3368 (2008). doi:10.1016/j.physd.2008.07.018
- [18] van Heijster, P., Doelman, A. and Kaper, T.J. Pinned fronts in heterogeneous media of jump type. Nonlinearity **24**(1) (2012). doi:10.1088/0951-7715/24/1/007
- [19] van Heijster, P., Doelman, A., Kaper, T.J. and Promislow, K. Front interactions in a three-component system. SIAM Journal on Applied Dynamical Systems **9**(2):292–332 (2010). doi:10.1137/080744785
- [20] Jaramillo, G. Inhomogeneities in 3 dimensional oscillatory media. Networks and Heterogeneous Media **10**(2):387–399 (2015). ISSN 1556-1801. doi:10.3934/nhm.2015.10.387. URL <https://www.aims sciences.org/article/id/0557cfc0-b939-46fa-a2e6-f30d3ae4cc81>
- [21] Jaramillo, G. Can large inhomogeneities generate target patterns? Zeitschrift für angewandte Mathematik und Physik **74**(4):134 (2023). doi:10.1007/s00033-023-02027-4
- [22] Jaramillo, G. and Scheel, A. Deformation of striped patterns by inhomogeneities. Mathematical Methods in the Applied Sciences **38**(1) (2015). doi:10.1002/mma.3049. URL <https://doi.org/10.1002/mma.3049>
- [23] Jaramillo, G., Scheel, A. and Wu, Q. The effect of impurities on striped phases. Proceedings of the Royal Society of Edinburgh Section A: Mathematics **149**(1):131–168 (2019). doi:10.1017/S0308210518000197
- [24] Kamphuis, J. and Chirilus-Bruckner, M. Pattern formation in a Swift-Hohenberg equation with spatially periodic coefficients. arXiv preprint (2025). doi:10.48550/arXiv.2506.22211. 2506.22211
- [25] Kollár, R. and Scheel, A. Coherent structures generated by inhomogeneities in oscillatory media. SIAM Journal on Applied Dynamical Systems **6**(2):236–262 (2007). doi:10.1137/060666950
- [26] Kolokolnikov, T. and Wei, J. Pattern formation in a reaction–diffusion system with space–dependent feed rate. SIAM Review **60**(3):626–645 (2018). doi:10.1137/17M1116027. Published electronically August 8, 2018
- [27] Krause, A.L., Klika, V., Villar-Sepúlveda, E., Champneys, A.R. and Gaffney, E.A. Pattern localisation in the Swift–Hohenberg equation via slowly varying spatial heterogeneity. SIAM Journal on Applied Dynamical Systems (2025). ISSN 1536-0040. Accepted July 11 2025; deposited in ORA July 12 2025
- [28] Krause, A.L., Klika, V., Woolley, T.E. and Gaffney, E.A. From one pattern into another: analysis of Turing patterns in heterogeneous domains via WKB. Journal of the Royal Society Interface **17**(169):20190621 (2020). doi:10.1098/rsif.2019.0621

- [29] Kuehn, C. and Sulzbach, J.E. Fast reactions and slow manifolds. Nonlinear Differential Equations and Applications **32**(72) (2025). doi:10.1007/s00030-025-01082-2. URL <https://doi.org/10.1007/s00030-025-01082-2>
- [30] Manor, R., Hagberg, A. and Meron, E. Wave-number locking in spatially forced pattern-forming systems. Europhysics Letters **83**(1):10005 (2008). doi:10.1209/0295-5075/83/10005
- [31] Mau, Y., Haim, L. and Meron, E. Reversing desertification as a spatial resonance problem. Physical Review E **91**(1):012903 (2015). doi:10.1103/PhysRevE.91.012903
- [32] Mielke, A. and Reichelt, S. Traveling fronts in a reaction-diffusion equation with a memory term. Journal of Dynamics and Differential Equations **36** (2024). doi:10.1007/s10884-022-10133-6. URL <https://doi.org/10.1007/s10884-022-10133-6>
- [33] Sandstede, B., Scheel, A. and Wulff, C. Dynamics of spiral waves on unbounded domains using center-manifold reductions. Journal of Differential Equations **141**(1):122–149 (1997). doi:10.1006/jdeq.1997.3326
- [34] Scheel, A. and Tikhomirov, S. Depinning asymptotics in ergodic media. In P. Gurevich, J. Hell, B. Sandstede and A. Scheel (eds.), Patterns of Dynamics, 88–108. Springer International Publishing, Cham (2017). ISBN 978-3-319-64173-7
- [35] Siero, E., Doelman, A., Eppinga, M.B., Rademacher, J.D.M., Rietkerk, M. and Siteur, K. Striped pattern selection by advective reaction-diffusion systems: Resilience of banded vegetation on slopes. Chaos: An Interdisciplinary Journal of Nonlinear Science **25**(3):036411 (2015). doi:10.1063/1.4914450. URL <https://doi.org/10.1063/1.4914450>
- [36] Soresina, C., Tang, B. and Tran, B.N. Fast-reaction limits for predator-prey reaction-diffusion systems: improved convergence. In M. Engel, H. Jardón-Kojakhmetov and C. Soresina (eds.), Topics in Multiple Time Scale Dynamics, vol. 806 of Contemporary Mathematics. American Mathematical Society (2024). ISBN 978-1-4704-7684-7. doi:10.1090/conm/806/16155. URL <https://www.ams.org/books/conm/806/16155>
- [37] Tang, B. and Tran, B.N. Rigorous derivation of Michaelis-Menten kinetics in the presence of slow diffusion. SIAM Journal on Mathematical Analysis **56**(5) (2024). doi:10.1137/23M1579406. URL <https://doi.org/10.1137/23M1579406>
- [38] Van Gorder, R.A. Pattern formation from spatially heterogeneous reaction-diffusion systems. Philosophical Transactions of the Royal Society A **379**(2213) (2021). doi:10.1098/rsta.2021.0001
- [39] van Vianen, L. Existence and dynamics of stationary and travelling fronts in a two component singularly perturbed RDE with spatial inhomogeneity. Ph.D. thesis, Leiden University (2025)
- [40] van Vianen, L. Laraleiden/code-numeric-examples: code-numeric-examples (2026). doi:10.5281/zenodo.18764472. URL <https://doi.org/10.5281/zenodo.18764472>
- [41] Wulff, C. Spiral waves and Euclidean symmetries. Zeitschrift für Physikalische Chemie **216**(4):535–558 (1998). doi:10.1524/zpch.2002.216.4.535